



ELSEVIER

Contents lists available at ScienceDirect

Applied and Computational Harmonic Analysis

www.elsevier.com/locate/acha



Spatiospectral concentration of vector fields on a sphere

Alain Plattner^{a,*}, Frederik J. Simons^{a,b}^a Department of Geosciences, Princeton University, Princeton, NJ 08544, USA^b Program in Applied and Computational Mathematics, Princeton University, Princeton, NJ 08544, USA

ARTICLE INFO

Article history:

Received 27 June 2012

Received in revised form 23 November 2012

Accepted 28 December 2012

Available online 3 January 2013

Communicated by G. Battle

Keywords:

Bandlimited function

Concentration problem

Eigenvalue problem

Spectral analysis

Vector spherical harmonics

ABSTRACT

We construct spherical vector bases that are bandlimited and spatially concentrated, or, alternatively, spacelimited and spectrally concentrated, suitable for the analysis and representation of real-valued vector fields on the surface of the unit sphere, as arises in the natural and biomedical sciences, and engineering. Building on the original approach of Slepian, Landau, and Pollak we concentrate the energy of our function bases into arbitrarily shaped regions of interest on the sphere, and within certain bandlimits in the vector spherical-harmonic domain. As with the concentration problem for scalar functions on the sphere, which has been treated in detail elsewhere, a Slepian vector basis can be constructed by solving a finite-dimensional algebraic eigenvalue problem. The eigenvalue problem decouples into separate problems for the radial and tangential components. For regions with advanced symmetry such as polar caps, the spectral concentration kernel matrix is very easily calculated and block-diagonal, lending itself to efficient diagonalization. The number of spatio-spectrally well-concentrated vector fields is well estimated by a Shannon number that only depends on the area of the target region and the maximal spherical-harmonic degree or bandwidth. The spherical Slepian vector basis is doubly orthogonal, both over the entire sphere and over the geographic target region. Like its scalar counterparts it should be a powerful tool in the inversion, approximation and extension of bandlimited fields on the sphere: vector fields such as gravity and magnetism in the earth and planetary sciences, or electromagnetic fields in optics, antenna theory and medical imaging.

© 2013 Elsevier Inc. All rights reserved.

1. Introduction

Since it is impossible to simultaneously bandlimit and spacelimit a function to a chosen region of interest, we need to resort to functions that are bandlimited but optimally concentrated, with respect to their spatial energy, inside a target region. Slepian, Landau, and Pollak presented the solution to the problem of optimally concentrating a signal in time and frequency in their seminal papers [1–4]. Their construction leads to a family of orthogonal taper functions that have been widely applied as windows to regularize the quadratic inverse problem of power-spectral estimation from time-series observations of finite extent [5]. The “Slepian functions”, as we shall be calling them, are furthermore of great utility as a basis for function representation, approximation, interpolation and extension, and to solve stochastic linear inverse problems in a wide range of disciplines. Several authors have studied the time-scale and time-frequency concentration problem in more general settings (see [6–8] and references therein for a review). More specifically, spherical scalar Slepian functions, spatially concentrated while bandlimited, or spectrally concentrated while spacelimited, have been applied in physical, computational, and biomedical fields such as geodesy [9–12] and gravimetry [13–17], geomagnetism [18,19] and geodynamics [20],

* Corresponding author.

E-mail address: plattner@alumni.ethz.ch (A. Plattner).

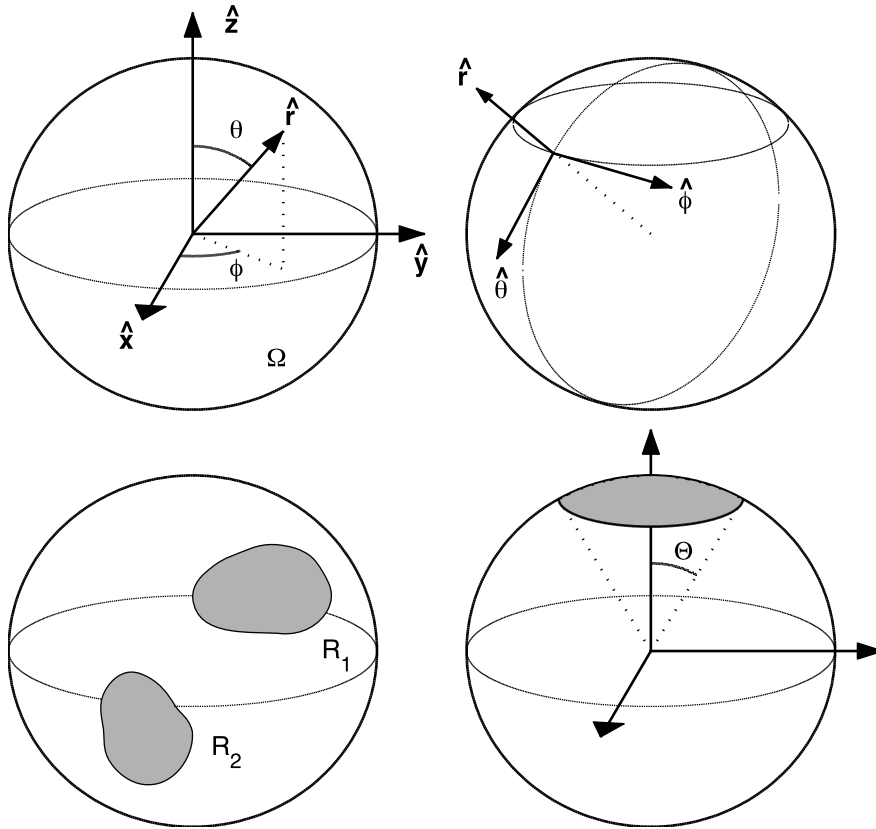


Fig. 1. Sketch illustrating the geometry of the vector spherical concentration problem. Lower right shows an axisymmetric polar cap of colatitudinal radius Θ as treated in Section 4. The area of the region of concentration, $R = R_1 \cup R_2 \cup \dots$, is denoted by A in the text.

planetary [21–24] and biomedical science [25,26], cosmology [27,28], and computer science [29,30], while continuing to be of interest in information and communication theory [31], signal processing [32,33], and mathematics [34,35].

To date only a few attempts have been made to bring the advantages of spherical Slepian functions into the realm of spherical vector fields. The first successful construction of spatially concentrated bandlimited tangential spherical vector fields was reported for applications in magnetoencephalography [25,26,36]. In geodesy, Eshagh [37] has developed methods to explicitly evaluate the product integrals arising in the concentration problem whose solutions are the vectorial Slepian functions. In this paper we present a complete extension of Slepian's spatio-spectral concentration problem to vector fields on the sphere, and give suggestions and examples as to their usage for problems of a geomagnetic nature (e.g. [38,39]). The family of optimally concentrated spherical vectorial multitapers that we will construct in the following should be useful in many scientific applications. In particular in geomagnetism, one of the objectives of the Swarm mission [40] is to model the lithospheric magnetic field with maximal resolution and accuracy, even in the presence of contaminating signals from secondary sources. In addition, and more generally, lithospheric-field data analysis will have to successfully merge information from the global to the regional scale. In the past decade or so, a variety of global-to-regional modeling techniques have come of age, including harmonic splines [41–43], stitching together local models [44–48], and wavelets [49–51]. Due to their optimal combination of spatial locality and spectral bandlimitation the basis functions constructed in this paper should be well suited to combine global and local data while respecting their bandlimitation.

2. Preliminaries

Fig. 1 shows the geometry of the unit sphere $\Omega = \{\hat{\mathbf{r}}: \|\hat{\mathbf{r}}\| = 1\}$ and its tangential vectors. The colatitude of spherical points $\hat{\mathbf{r}}$ is denoted by $0 \leq \theta \leq \pi$ and the longitude by $0 \leq \phi < 2\pi$; we denote the unit vector pointing outwards in the radial direction by $\hat{\mathbf{r}}$, and the unit vectors in the tangential directions towards the south pole and towards the east will be denoted by $\hat{\theta}$ and $\hat{\phi}$, respectively. The symbol R will be used to denote a region of the unit sphere Ω , of area $A = \int_R d\Omega$, within which the bandlimited vector field shall be concentrated. The region can be a combination of disjoint subregions, $R = R_1 \cup R_2 \cup \dots$, and the boundaries of those subregions can be irregularly shaped, as depicted. We will denote the region complementary to R by $\Omega \setminus R$.

2.1. Real scalar spherical harmonics

Restricting our attention to real-valued vector fields, we use real vector spherical harmonics, which are constructed from their scalar counterparts. Each scalar spherical harmonic Y_{lm} has a degree $0 \leq l$ and, for each degree, an order $-l \leq m \leq l$. Our spherical harmonics are unit-normalized in the sense [52]

$$Y_{lm}(\theta, \phi) = \begin{cases} \sqrt{2}X_{l|m|}(\theta) \cos m\phi & \text{if } -l \leq m < 0, \\ X_{l0}(\theta) & \text{if } m = 0, \\ \sqrt{2}X_{lm}(\theta) \sin m\phi & \text{if } 0 < m \leq l, \end{cases} \tag{1}$$

$$X_{lm}(\theta) = (-1)^m \left(\frac{2l+1}{4\pi}\right)^{1/2} \left[\frac{(l-m)!}{(l+m)!}\right]^{1/2} P_{lm}(\cos \theta), \tag{2}$$

$$P_{lm}(\mu) = \frac{1}{2^l l!} (1-\mu^2)^{m/2} \left(\frac{d}{d\mu}\right)^{l+m} (\mu^2-1)^l. \tag{3}$$

The asymptotic wavenumber associated with a harmonic degree l is $\sqrt{l(l+1)}$ [53]. The function $P_{lm}(\mu)$ in (3) is called the associated Legendre function of integer degree l and order m . The spherical harmonics $Y_{lm}(\hat{\mathbf{r}})$ are eigenfunctions of the Laplace–Beltrami operator, $\nabla_1^2 Y_{lm} = -l(l+1)Y_{lm}$, where $\nabla_1^2 = \partial_\theta^2 + \cot \theta \partial_\theta + (\sin \theta)^{-2} \partial_\phi^2$. We choose the constants in (1)–(3) to guarantee orthonormality:

$$\int_{\Omega} Y_{lm} Y_{l'm'} d\Omega = \delta_{ll'} \delta_{mm'}. \tag{4}$$

The product of two normalized Legendre functions [52,54] is the linear combination

$$X_{lm}(\theta) X_{l'm'}(\theta) = (-1)^{m+m'} \sum_{n=|l-l'|}^{l+l'} \sqrt{\frac{(2n+1)(2l+1)(2l'+1)}{4\pi}} \begin{pmatrix} l & n & l' \\ 0 & 0 & 0 \end{pmatrix} \begin{pmatrix} l & n & l' \\ m & -m & m' \end{pmatrix} X_{nm+m'}(\theta). \tag{5}$$

The index arrays in (5) are Wigner 3- j symbols [54,55]. We will use the following two recursion relations [37,56] for the derivatives of the $X_{lm}(\theta)$ and their divisions by $\sin \theta$. Define

$$X'_{lm} = \frac{dX_{lm}}{d\theta}. \tag{6}$$

Then, from the work by Ilk [56] it follows that, for $0 \leq l$ and $0 \leq m \leq l$,

$$X'_{lm} = a_{lm}^- X_{l,m-1} + a_{lm}^+ X_{l,m+1}, \tag{7}$$

where

$$a_{lm}^\pm = \pm \frac{\sqrt{(l \mp m)(l \pm m + 1)}}{2}, \tag{8}$$

and, for $0 \leq l$ and $1 \leq m \leq l$,

$$(\sin \theta)^{-1} m X_{lm} = b_{lm}^- X_{l-1,m-1} + b_{lm}^+ X_{l-1,m+1}, \tag{9}$$

where

$$b_{lm}^\pm = -\sqrt{\frac{2l+1}{2l-1}} \frac{\sqrt{(l \mp m)(l \mp m - 1)}}{2}. \tag{10}$$

In both (7) and (9), for $l < 0$, or $m < 0$, or $l < m$, we have $X_{lm} = 0$.

Finally, as shown by Paul [57], integrals of the type

$$I_{lm}(\Theta) = \int_0^\Theta X_{lm}(\theta) \sin \theta d\theta \tag{11}$$

can be exactly evaluated recursively. When $l \geq 2$ and $0 \leq m < l$, we have

$$I_{lm}(\Theta) = \frac{l-2}{l+1} \sqrt{\frac{(2l+1)[(l-1)^2 - m^2]}{(2l-3)(l^2 - m^2)}} I_{l-2,m}(\Theta) + \frac{1}{l+1} \sqrt{\frac{4l^2 - 1}{l^2 - m^2}} \sin^2 \Theta X_{l-1,m}(\Theta), \tag{12}$$

and, for $l \geq 2$ and $m = l$, the formula

$$I_{ll}(\Theta) = \frac{1}{l+1} \sqrt{\frac{2l+1}{4l^2-4l}} [l\sqrt{2l-1}I_{l-2l-2}(\Theta) - (\sin \Theta)^2 X_{l-1l-2}(\Theta)]. \quad (13)$$

The recursions (12)–(13) are to be started from

$$\begin{aligned} X_{00}(\Theta) &= \frac{1}{2\sqrt{\pi}}, & I_{00}(\Theta) &= \frac{1}{2\sqrt{\pi}}(1 - \cos \Theta), \\ X_{10}(\Theta) &= \frac{1}{2}\sqrt{\frac{3}{\pi}} \cos \Theta, & I_{10}(\Theta) &= \frac{1}{4}\sqrt{\frac{3}{\pi}}(\sin \Theta)^2, \\ X_{11}(\Theta) &= -\frac{1}{2}\sqrt{\frac{3}{2\pi}} \sin \Theta, & I_{11}(\Theta) &= -\frac{1}{4}\sqrt{\frac{3}{2\pi}}(\Theta - \sin 2\Theta), \end{aligned} \quad (14)$$

hence enabling the exact evaluation of all integrals $I_{lm}(\Theta)$ for $l \geq 0$ and $0 \leq m \leq l$.

2.2. Real-valued vector spherical harmonics

The canonical three-dimensional gradient operator $\nabla = \hat{\mathbf{x}}\partial_x + \hat{\mathbf{y}}\partial_y + \hat{\mathbf{z}}\partial_z$ can be expressed as [52]

$$\nabla = \hat{\mathbf{r}}\partial_r + r^{-1}\nabla_1, \quad \text{where } \nabla_1 = \hat{\boldsymbol{\theta}}\partial_\theta + \hat{\boldsymbol{\phi}}(\sin \theta)^{-1}\partial_\phi. \quad (15)$$

For any differentiable function $H(\hat{\mathbf{r}})$ on the unit sphere, the vector field $\hat{\mathbf{r}}H(\hat{\mathbf{r}})$ is purely radial, the vector fields $\nabla_1 H(\hat{\mathbf{r}})$ and $\hat{\mathbf{r}} \times \nabla_1 H(\hat{\mathbf{r}})$ are purely tangential, and all three are mutually orthogonal. We can thus construct vector spherical harmonics from gradients of scalar spherical harmonics by defining, for $l > 0$ and $-m \leq l \leq m$,

$$\mathbf{P}_{lm} = \hat{\mathbf{r}}Y_{lm}, \quad (16)$$

$$\mathbf{B}_{lm} = \frac{\nabla_1 Y_{lm}}{\sqrt{l(l+1)}} = \frac{[\hat{\boldsymbol{\theta}}\partial_\theta + \hat{\boldsymbol{\phi}}(\sin \theta)^{-1}\partial_\phi]Y_{lm}}{\sqrt{l(l+1)}}, \quad (17)$$

$$\mathbf{C}_{lm} = \frac{-\hat{\mathbf{r}} \times \nabla_1 Y_{lm}}{\sqrt{l(l+1)}} = \frac{[\hat{\boldsymbol{\theta}}(\sin \theta)^{-1}\partial_\phi - \hat{\boldsymbol{\phi}}\partial_\theta]Y_{lm}}{\sqrt{l(l+1)}}, \quad (18)$$

together with the purely radial $\mathbf{P}_{00} = (4\pi)^{-1/2}\hat{\mathbf{r}}$ and the vanishing $\mathbf{B}_{00} = \mathbf{C}_{00} = \mathbf{0}$. The orthonormality of $\hat{\mathbf{r}}$, $\hat{\boldsymbol{\theta}}$, and $\hat{\boldsymbol{\phi}}$ immediately leads to

$$\mathbf{P}_{lm} \cdot \mathbf{B}_{l'm'} = \mathbf{P}_{lm} \cdot \mathbf{C}_{l'm'} = \mathbf{0}, \quad (19)$$

and the vector spherical harmonics are furthermore orthonormal in the sense

$$\begin{aligned} \int_{\Omega} \mathbf{P}_{lm} \cdot \mathbf{P}_{l'm'} d\Omega &= \int_{\Omega} \mathbf{B}_{lm} \cdot \mathbf{B}_{l'm'} d\Omega = \int_{\Omega} \mathbf{C}_{lm} \cdot \mathbf{C}_{l'm'} d\Omega = \delta_{ll'} \delta_{mm'}, \\ \int_{\Omega} \mathbf{P}_{lm} \cdot \mathbf{B}_{l'm'} d\Omega &= \int_{\Omega} \mathbf{P}_{lm} \cdot \mathbf{C}_{l'm'} d\Omega = \int_{\Omega} \mathbf{B}_{lm} \cdot \mathbf{C}_{l'm'} d\Omega = 0. \end{aligned} \quad (20)$$

The vector spherical-harmonic addition theorem [58] comprises the identities

$$\sum_{m=-l}^l \mathbf{P}_{lm}(\hat{\mathbf{r}}) \cdot \mathbf{P}_{lm}(\hat{\mathbf{r}}) = \left(\frac{2l+1}{4\pi}\right) = \sum_{m=-l}^l \mathbf{B}_{lm}(\hat{\mathbf{r}}) \cdot \mathbf{B}_{lm}(\hat{\mathbf{r}}) = \sum_{m=-l}^l \mathbf{C}_{lm}(\hat{\mathbf{r}}) \cdot \mathbf{C}_{lm}(\hat{\mathbf{r}}). \quad (21)$$

2.3. Real-valued vector fields on the unit sphere

The expansion of a real-valued square-integrable vector field \mathbf{u} on the unit sphere Ω can be written as

$$\mathbf{u} = \sum_{lm} U_{lm} \mathbf{P}_{lm} + V_{lm} \mathbf{B}_{lm} + W_{lm} \mathbf{C}_{lm}, \quad (22)$$

where the expansion coefficients are obtained via

$$U_{lm} = \int_{\Omega} \mathbf{P}_{lm} \cdot \mathbf{u} d\Omega, \quad V_{lm} = \int_{\Omega} \mathbf{B}_{lm} \cdot \mathbf{u} d\Omega \quad \text{and} \quad W_{lm} = \int_{\Omega} \mathbf{C}_{lm} \cdot \mathbf{u} d\Omega, \quad (23)$$

and using the shorthand notation $\sum_{lm}^L := \sum_{l=0}^L \sum_{m=-l}^l$ when \mathbf{P}_{lm} or U_{lm} are involved, and $\sum_{lm}^L := \sum_{l=1}^L \sum_{m=-l}^l$, for \mathbf{B}_{lm} , \mathbf{C}_{lm} , V_{lm} or W_{lm} . A sans serif \mathbf{u} will be used to denote the ordered column vector of vector spherical-harmonic coefficients, namely $\mathbf{u} = (\dots, U_{lm}, \dots, V_{lm}, \dots, W_{lm}, \dots)^T$. We will denote the norms of a spatial-domain vector field $\mathbf{u}(\hat{\mathbf{r}})$ and its spectral-domain equivalent \mathbf{u} by

$$\|\mathbf{u}\|_{\Omega}^2 = \int_{\Omega} \mathbf{u} \cdot \mathbf{u} d\Omega, \quad \|\mathbf{u}\|_{\infty}^2 = \sum_{lm}^{\infty} U_{lm}^2 + V_{lm}^2 + W_{lm}^2. \tag{24}$$

Hence Parseval’s relation can be written in the form $\|\mathbf{u}\|_{\Omega}^2 = \|\mathbf{u}\|_{\infty}^2$. Any square-integrable vector field \mathbf{u} on the sphere can be decomposed into a radial component, \mathbf{u}^r , and a tangential component, \mathbf{u}^t , thus $\mathbf{u} = \mathbf{u}^r + \mathbf{u}^t$, whereby

$$\mathbf{u}^r = \sum_{lm}^{\infty} U_{lm} \mathbf{P}_{lm} \quad \text{and} \quad \mathbf{u}^t = \sum_{lm}^{\infty} V_{lm} \mathbf{B}_{lm} + W_{lm} \mathbf{C}_{lm}. \tag{25}$$

We use $\delta(\hat{\mathbf{r}}, \hat{\mathbf{r}}')$ for the vector Dirac delta function on the sphere. Accordingly,

$$\int_{\Omega} \delta(\hat{\mathbf{r}}, \hat{\mathbf{r}}') \cdot \mathbf{u}(\hat{\mathbf{r}}) d\Omega = \mathbf{u}(\hat{\mathbf{r}}'). \tag{26}$$

The vector spherical-harmonic representation of $\delta(\hat{\mathbf{r}}, \hat{\mathbf{r}}')$ is the sum of dyads

$$\delta(\hat{\mathbf{r}}, \hat{\mathbf{r}}') = \sum_{lm}^{\infty} \mathbf{P}_{lm}(\hat{\mathbf{r}}) \mathbf{P}_{lm}(\hat{\mathbf{r}}') + \mathbf{B}_{lm}(\hat{\mathbf{r}}) \mathbf{B}_{lm}(\hat{\mathbf{r}}') + \mathbf{C}_{lm}(\hat{\mathbf{r}}) \mathbf{C}_{lm}(\hat{\mathbf{r}}'). \tag{27}$$

2.4. Bandlimited and spacelimited vector fields

We shall now consider two subspaces of the space of all square-integrable vector fields on the unit sphere Ω . Given $\mathbf{g} = (\dots, U_{lm}, \dots, V_{lm}, \dots, W_{lm}, \dots)^T$, we define the space of all bandlimited vector fields $\mathcal{S}_L = \{\mathbf{g}: U_{lm} = V_{lm} = W_{lm} = 0 \text{ for } L < l \leq \infty \text{ and } -l \leq m \leq l\}$, with no power beyond the bandwidth L , whose elements are the functions

$$\mathbf{g} = \mathbf{g}^r + \mathbf{g}^t = \sum_{lm}^L U_{lm} \mathbf{P}_{lm} + V_{lm} \mathbf{B}_{lm} + W_{lm} \mathbf{C}_{lm}, \tag{28}$$

where now

$$U_{lm} = \int_{\Omega} \mathbf{P}_{lm} \cdot \mathbf{g} d\Omega, \quad V_{lm} = \int_{\Omega} \mathbf{B}_{lm} \cdot \mathbf{g} d\Omega, \quad \text{and} \quad W_{lm} = \int_{\Omega} \mathbf{C}_{lm} \cdot \mathbf{g} d\Omega. \tag{29}$$

Similarly, we define $\mathcal{S}_R = \{\mathbf{h}: \mathbf{h} = \mathbf{0} \text{ in } \Omega \setminus R\}$ to be the space of all spacelimited vector fields $\mathbf{h}(\hat{\mathbf{r}})$ that are equal to zero outside a non-empty region $R \subset \Omega$. By definition, the space \mathcal{S}_R is infinite-dimensional but $\dim \mathcal{S}_L = 3(L + 1)^2 - 2$, because the coefficient vector \mathbf{g} has $\sum_{l=0}^L (2l + 1) = (L + 1)^2$ entries for the U_{lm} and $\sum_{l=1}^L (2l + 1) = (L + 1)^2 - 1$ entries for the V_{lm} and W_{lm} , respectively. We define the spatial and spectral measures analogously to (24)

$$\|\mathbf{g}\|_R^2 = \int_R \mathbf{g} \cdot \mathbf{g} d\Omega, \quad \|\mathbf{g}\|_L^2 = \sum_{lm}^L U_{lm}^2 + V_{lm}^2 + W_{lm}^2. \tag{30}$$

3. Concentration within an arbitrarily shaped region

No vector field can be strictly bandlimited and strictly spacelimited, i.e., no $\mathbf{u}(\hat{\mathbf{r}})$ can simultaneously be contained in both spaces \mathcal{S}_R and \mathcal{S}_L . Our goal is to determine bandlimited vector fields $\mathbf{g}(\hat{\mathbf{r}}) \in \mathcal{S}_L$ with optimal energy-concentration within a spatial region R , and those spacelimited vector fields $\mathbf{h}(\hat{\mathbf{r}}) \in \mathcal{S}_R$ with a spectrum optimally concentrated within an interval $0 \leq l \leq L$. Similar to the scalar time-frequency [1], multidimensional Cartesian [6,59] and spherical [7] cases, these two spatio-spectral concentration problems are closely related.

3.1. Spatial concentration of bandlimited vector fields

We maximize the spatial concentration of a bandlimited vector field $\mathbf{g}(\hat{\mathbf{r}}) \in \mathcal{S}_L$ within R via the ratio

$$\lambda = \frac{\|\mathbf{g}\|_R^2}{\|\mathbf{g}\|_{\Omega}^2} = \frac{\int_R \mathbf{g} \cdot \mathbf{g} d\Omega}{\int_{\Omega} \mathbf{g} \cdot \mathbf{g} d\Omega} = \text{maximum}. \tag{31}$$

The variational problem (31) is analogous to that encountered in one and two scalar dimensions. As there, the energy ratio $0 < \lambda < 1$ is a measure of the spatial concentration.

3.1.1. Purely radial vector fields

As a first step, we focus on solving (31) for purely radial fields, that is, bandlimited vector fields in the decomposition (25),

$$\mathbf{g}^r = \sum_{lm}^L U_{lm} \mathbf{P}_{lm}. \quad (32)$$

To simplify the notation we drop the superscript on the coefficient vector, such that $\mathbf{g} = (\dots, U_{lm}, \dots)^T$ in this section. Inserting the representation (32) into (31) and switching the order of summation and integration, we can express λ as

$$\lambda = \frac{\sum_{lm}^L U_{lm} \sum_{l'm'}^L P_{lm,l'm'} U_{l'm'}}{\sum_{lm}^L U_{lm}^2}. \quad (33)$$

Here we have used orthonormality (20) and defined the quantities

$$P_{lm,l'm'} = \int_R \mathbf{P}_{lm} \cdot \mathbf{P}_{l'm'} d\Omega = \int_R Y_{lm} Y_{l'm'} d\Omega. \quad (34)$$

We can reformulate (31) as a matrix variational problem [60]:

$$\lambda = \frac{\mathbf{g}^T \mathbf{P} \mathbf{g}}{\mathbf{g}^T \mathbf{g}} = \text{maximum}, \quad (35)$$

using the $(L+1)^2 \times (L+1)^2$ matrix

$$\mathbf{P} = \begin{pmatrix} P_{00,00} & \cdots & P_{00,LL} \\ \vdots & & \vdots \\ P_{LL,00} & \cdots & P_{LL,LL} \end{pmatrix}. \quad (36)$$

The stationary solutions of the Rayleigh quotient λ in (35) are solutions of the $(L+1)^2 \times (L+1)^2$ algebraic eigenvalue problem

$$\mathbf{P} \mathbf{g} = \lambda \mathbf{g}. \quad (37)$$

Therefore the spatial concentration problem of purely radial bandlimited vector fields is completely equivalent to the scalar spherical concentration problem [7].

3.1.2. General vector fields

For bandlimited vector fields that are of the kind (28), and therefore described by the complete coefficient vector $\mathbf{g} = (\dots, U_{lm}, \dots, V_{lm}, \dots, W_{lm}, \dots)^T$, operations analogous to those carried out in Section 3.1.1 transform (31) into a matrix variational problem in the space of $[3(L+1)^2 - 2]$ -tuples:

$$\lambda = \frac{\mathbf{g}^T \mathbf{K} \mathbf{g}}{\mathbf{g}^T \mathbf{g}} = \text{maximum}. \quad (38)$$

Since the inner products of \mathbf{P}_{lm} with \mathbf{B}_{lm} and \mathbf{C}_{lm} are always zero because of (19),

$$\mathbf{K} = \begin{pmatrix} \mathbf{P} & \mathbf{0} & \mathbf{0} \\ \mathbf{0} & \mathbf{B} & \mathbf{D} \\ \mathbf{0} & \mathbf{D}^T & \mathbf{C} \end{pmatrix} = \begin{pmatrix} \mathbf{P} & \mathbf{0} \\ \mathbf{0} & \mathbf{Q} \end{pmatrix}, \quad (39)$$

where the $[(L+1)^2 - 1] \times [(L+1)^2 - 1]$ -dimensional matrices cycle through all applicable degrees and orders

$$\mathbf{B} = \begin{pmatrix} B_{10,10} & \cdots & B_{10,LL} \\ \vdots & & \vdots \\ B_{LL,10} & \cdots & B_{LL,LL} \end{pmatrix}, \quad (40)$$

$$\mathbf{C} = \begin{pmatrix} C_{10,10} & \cdots & C_{10,LL} \\ \vdots & & \vdots \\ C_{LL,10} & \cdots & C_{LL,LL} \end{pmatrix}, \quad (41)$$

$$\mathbf{D} = \begin{pmatrix} D_{10,10} & \cdots & D_{10,LL} \\ \vdots & & \vdots \\ D_{LL,10} & \cdots & D_{LL,LL} \end{pmatrix}, \quad (42)$$

have matrix entries defined by

$$B_{lm,l'm'} = \int_R \mathbf{B}_{lm} \cdot \mathbf{B}_{l'm'} d\Omega, \tag{43}$$

$$C_{lm,l'm'} = \int_R \mathbf{C}_{lm} \cdot \mathbf{C}_{l'm'} d\Omega, \tag{44}$$

$$D_{lm,l'm'} = \int_R \mathbf{B}_{lm} \cdot \mathbf{C}_{l'm'} d\Omega, \tag{45}$$

and

$$\mathbf{Q} = \begin{pmatrix} \mathbf{B} & \mathbf{D} \\ \mathbf{D}^T & \mathbf{C} \end{pmatrix} = \begin{pmatrix} \mathbf{B} & \mathbf{D} \\ -\mathbf{D} & \mathbf{B} \end{pmatrix}. \tag{46}$$

The last identity follows from (17)–(18) and (43)–(45). The solutions to the concentration problem of general bandlimited vector fields to arbitrary domains solve the $[3(L+1)^2 - 2] \times [3(L+1)^2 - 2]$ -dimensional algebraic eigenvalue problem

$$\mathbf{K}\mathbf{g} = \lambda\mathbf{g}. \tag{47}$$

The matrix (39) is real, symmetric ($\mathbf{K}^T = \mathbf{K}$), and it is positive definite ($\mathbf{g}^T \mathbf{K} \mathbf{g} > 0$ for all $\mathbf{g} \neq 0$), hence the $3(L+1)^2 - 2$ eigenvalues λ and associated eigenvectors \mathbf{g} are always real. The eigenvalues $\lambda_1, \lambda_2, \dots, \lambda_{3(L+1)^2-2}$ and eigenvectors $\mathbf{g}_1, \mathbf{g}_2, \dots, \mathbf{g}_{3(L+1)^2-2}$ can be ordered so that they are sorted $1 > \lambda_1 \geq \lambda_2 \geq \dots \geq \lambda_{3(L+1)^2-2} > 0$. Every spectral-domain eigenvector \mathbf{g}_α is associated with a bandlimited spatial eigenfield $\mathbf{g}_\alpha(\hat{\mathbf{r}})$ defined by (28). If R is a true subset of Ω , then the largest eigenvalue, λ_1 , will be strictly smaller than one since no bandlimited function can be non-zero only within a region R that is smaller than Ω . Due to the positive definiteness of the matrix \mathbf{K} for a non-empty region R , the smallest eigenvalue, $\lambda_{3(L+1)^2-2}$, is larger than zero.

The eigenvectors $\mathbf{g}_1, \mathbf{g}_2, \dots, \mathbf{g}_{3(L+1)^2-2}$ are orthogonal. We orthonormalize them as

$$\mathbf{g}_\alpha^T \mathbf{g}_\beta = \delta_{\alpha\beta}, \quad \mathbf{g}_\alpha^T \mathbf{K} \mathbf{g}_\beta = \lambda_\alpha \delta_{\alpha\beta}. \tag{48}$$

The associated eigenfields $\mathbf{g}_1(\hat{\mathbf{r}}), \mathbf{g}_2(\hat{\mathbf{r}}), \dots, \mathbf{g}_{3(L+1)^2-2}(\hat{\mathbf{r}})$ are a basis for \mathcal{S}_L that is orthogonal over the region R and orthonormal over the whole sphere Ω :

$$\int_\Omega \mathbf{g}_\alpha \cdot \mathbf{g}_\beta d\Omega = \delta_{\alpha\beta}, \quad \int_R \mathbf{g}_\alpha \cdot \mathbf{g}_\beta d\Omega = \lambda_\alpha \delta_{\alpha\beta}. \tag{49}$$

The relations (49) for the spatial domain are equivalent to their matrix counterparts (48). The eigenfield $\mathbf{g}_1(\hat{\mathbf{r}})$ with the largest eigenvalue λ_1 is the element in the space \mathcal{S}_L of bandlimited vector fields with most of its spatial energy within region R ; the eigenfield $\mathbf{g}_2(\hat{\mathbf{r}})$ is the next best-concentrated element in \mathcal{S}_L that is orthogonal to $\mathbf{g}_1(\hat{\mathbf{r}})$ over both Ω and R ; and so on.

When expressed in index notation, the eigenvalue equations (47) are

$$\sum_{l'm'}^L P_{lm,l'm'} U_{l'm'} = \lambda U_{lm}, \tag{50}$$

$$\sum_{l'm'}^L B_{lm,l'm'} V_{l'm'} + D_{lm,l'm'} W_{l'm'} = \lambda V_{lm}, \tag{51}$$

$$\sum_{l'm'}^L D_{lm,l'm'}^T V_{l'm'} + C_{lm,l'm'} W_{l'm'} = \lambda W_{lm}. \tag{52}$$

By tensor-multiplying the expression (50) with $\mathbf{P}_{lm}(\hat{\mathbf{r}})$, (51) with $\mathbf{B}_{lm}(\hat{\mathbf{r}})$, and (52) with $\mathbf{C}_{lm}(\hat{\mathbf{r}})$, and summing in each equation over all $0 \leq l \leq L$ and $-l \leq m \leq l$, we obtain the following system of spatial-domain equations:

$$\int_R \left[\sum_{lm}^L \mathbf{P}_{lm}(\hat{\mathbf{r}}) \mathbf{P}_{lm}(\hat{\mathbf{r}}') \right] \cdot \mathbf{g}^t(\hat{\mathbf{r}}') d\Omega' = \lambda \mathbf{g}^t(\hat{\mathbf{r}}), \tag{53}$$

$$\int_R \left[\sum_{lm}^L \mathbf{B}_{lm}(\hat{\mathbf{r}}) \mathbf{B}_{lm}(\hat{\mathbf{r}}') \right] \cdot \mathbf{g}^t(\hat{\mathbf{r}}') d\Omega' = \lambda \sum_{lm}^L V_{lm} \mathbf{B}_{lm}(\hat{\mathbf{r}}), \tag{54}$$

$$\int_R \left[\sum_{lm}^L \mathbf{C}_{lm}(\hat{\mathbf{r}}) \mathbf{C}_{lm}(\hat{\mathbf{r}}') \right] \cdot \mathbf{g}^t(\hat{\mathbf{r}}') d\Omega' = \lambda \sum_{lm}^L W_{lm} \mathbf{C}_{lm}(\hat{\mathbf{r}}). \quad (55)$$

By adding Eqs. (53)–(55), we obtain the spatial-domain eigenvalue problem

$$\int_R \mathbf{K}(\hat{\mathbf{r}}, \hat{\mathbf{r}}') \cdot \mathbf{g}(\hat{\mathbf{r}}') d\Omega' = \lambda \mathbf{g}(\hat{\mathbf{r}}), \quad \hat{\mathbf{r}} \in \Omega, \quad (56)$$

a Fredholm integral equation [61] with a finite-rank, symmetric, separable, bandlimited vector Dirac delta function kernel,

$$\mathbf{K}(\hat{\mathbf{r}}, \hat{\mathbf{r}}') = \sum_{lm}^L \mathbf{P}_{lm}(\hat{\mathbf{r}}) \mathbf{P}_{lm}(\hat{\mathbf{r}}') + \mathbf{B}_{lm}(\hat{\mathbf{r}}) \mathbf{B}_{lm}(\hat{\mathbf{r}}') + \mathbf{C}_{lm}(\hat{\mathbf{r}}) \mathbf{C}_{lm}(\hat{\mathbf{r}}'), \quad (57)$$

a reproducing kernel [6,8] in the space S_L . By inserting the representations (28) and (57) into (56), we obtain again the matrix equation (47). Therefore the spectral-domain eigenvalue problem for \mathbf{g} and the spatial-domain eigenvalue problem for a bandlimited $\mathbf{g}(\hat{\mathbf{r}}) \in S_L$ are completely equivalent.

In summary, it is possible to construct an orthogonal family of bandlimited eigenfields that is optimally concentrated within a region R on the unit sphere Ω , by solving either the Fredholm integral equation (56) for the associated spatial-domain eigenfields $\mathbf{g}_1, \mathbf{g}_2, \dots, \mathbf{g}_{3(L+1)^2-2}$ or the matrix eigenvalue problem (47) for spectral-domain eigenvectors $\mathbf{g}_1, \mathbf{g}_2, \dots, \mathbf{g}_{3(L+1)^2-2}$. Both methods determine the optimally concentrated eigenfields over the complete domain Ω , i.e., both in the region R , within which they are concentrated, and in the complementary region $\Omega \setminus R$, into which they show inevitable leakage.

3.2. Spectral concentration of spacelimited vector fields

Instead of energy-concentrating a bandlimited vector field $\mathbf{g}(\hat{\mathbf{r}}) \in S_L$ within a spatial region R , we may choose to construct a spacelimited vector field $\mathbf{h}(\hat{\mathbf{r}}) \in S_R$ that is concentrated within the spectral interval $0 \leq l \leq L < \infty$. Such a spacelimited vector function will be defined by

$$\mathbf{h} = \sum_{lm}^{\infty} U'_{lm} \mathbf{P}_{lm} + V'_{lm} \mathbf{B}_{lm} + W'_{lm} \mathbf{C}_{lm}, \quad (58)$$

with the expansion coefficients given by the spatially limited integrals

$$U'_{lm} = \int_R \mathbf{P}_{lm} \cdot \mathbf{h} d\Omega, \quad V'_{lm} = \int_R \mathbf{B}_{lm} \cdot \mathbf{h} d\Omega \quad \text{and} \quad W'_{lm} = \int_R \mathbf{C}_{lm} \cdot \mathbf{h} d\Omega. \quad (59)$$

The quadratic concentration measure analogous to (31) is now the ratio

$$\lambda = \frac{\|\mathbf{h}\|_L^2}{\|\mathbf{h}\|_{\infty}^2} = \frac{\sum_{lm}^L U_{lm}'^2 + V_{lm}'^2 + W_{lm}'^2}{\sum_{lm}^{\infty} U_{lm}'^2 + V_{lm}'^2 + W_{lm}'^2} = \text{maximum}. \quad (60)$$

The variational problem (60) can once again be rewritten as a Rayleigh quotient,

$$\lambda = \frac{\int_R \int_R \mathbf{h}(\hat{\mathbf{r}}) \cdot \mathbf{K}(\hat{\mathbf{r}}, \hat{\mathbf{r}}') \cdot \mathbf{h}(\hat{\mathbf{r}}') d\Omega d\Omega'}{\int_R \mathbf{h}(\hat{\mathbf{r}}) \cdot \mathbf{h}(\hat{\mathbf{r}}) d\Omega} = \text{maximum}, \quad (61)$$

by inserting the vector spherical-harmonic expansion coefficients (59) into (60), switching the order of summation and integration, and by making use of the reproducing property (26) of the delta function (27) and the definition (57) of the kernel $\mathbf{K}(\hat{\mathbf{r}}, \hat{\mathbf{r}}')$. Stationary solutions of (60) solve the Fredholm integral equation

$$\int_R \mathbf{K}(\hat{\mathbf{r}}, \hat{\mathbf{r}}') \cdot \mathbf{h}(\hat{\mathbf{r}}') d\Omega' = \lambda \mathbf{h}(\hat{\mathbf{r}}), \quad \hat{\mathbf{r}} \in R. \quad (62)$$

This equation for $\mathbf{h}(\hat{\mathbf{r}}) \in S_R$ is identical to (56) for $\mathbf{g}(\hat{\mathbf{r}}) \in S_L$, the difference being that (56) is applicable on the entire sphere Ω , while the domain of (62) is limited to the region R , within which $\mathbf{h}(\hat{\mathbf{r}}) \neq \mathbf{0}$. We constructed the spectral norm ratio maximizing eigenfields $\mathbf{h}(\hat{\mathbf{r}})$ for (60) such that they are identical to the eigenfields $\mathbf{g}(\hat{\mathbf{r}})$ that maximize the spatial norm ratio (31) within the region R . We normalize such that

$$\mathbf{h}(\hat{\mathbf{r}}) = \begin{cases} \mathbf{g}(\hat{\mathbf{r}}) & \text{if } \hat{\mathbf{r}} \in R, \\ \mathbf{0} & \text{otherwise.} \end{cases} \quad (63)$$

Every bandlimited eigenfield $\mathbf{g}_\alpha \in \mathcal{S}_L$ leads to a spacelimited $\mathbf{h}_\alpha \in \mathcal{S}_R$ by the restriction (63). The eigenvalues λ_α associated with the corresponding \mathbf{g}_α measure the fractional spatial energy $1 - \lambda_\alpha$ that leaks to the region $\Omega \setminus R$. These eigenvalues are identical to the fractional spectral energy that leaks into the degrees $L < l \leq \infty$ by truncating \mathbf{g}_α in the construction of \mathbf{h}_α (63). Equivalently, we could have started with the variational problem (60) instead of (31) to obtain the integral equation (56) and then extended the domain (62) to the whole sphere Ω .

The spacelimited eigenfields $\mathbf{h}_1(\hat{\mathbf{r}}), \mathbf{h}_2(\hat{\mathbf{r}}), \dots, \mathbf{h}_{3(L+1)^2-2}$ constructed from (63) are orthogonal over both the whole sphere Ω and the region R :

$$\int_{\Omega} \mathbf{h}_\alpha \cdot \mathbf{h}_\beta \, d\Omega = \int_R \mathbf{h}_\alpha \cdot \mathbf{h}_\beta \, d\Omega = \lambda_\alpha \delta_{\alpha\beta}. \tag{64}$$

We can express the expansion coefficients of $\mathbf{h} = (\dots, U'_{lm}, \dots, V'_{lm}, \dots, W'_{lm}, \dots)^T$, where $0 \leq l \leq \infty$, by the coefficients $\mathbf{g} = (\dots, U_{lm}, \dots, V_{lm}, \dots, W_{lm}, \dots)^T$, with $0 \leq l \leq L$, using the relation $\mathbf{h} = \mathbf{K}\mathbf{g}$, which leads to $U'_{lm} = \lambda U_{lm}$, $V'_{lm} = \lambda V_{lm}$ and $W'_{lm} = \lambda W_{lm}$, when $0 \leq l \leq L$, due to (50)–(52). The solutions to Eq. (62) form an infinite-dimensional space. The complement to the $3(L+1)^2 - 2$ eigenfields with non-zero eigenvalues $\lambda_1, \lambda_2, \dots, \lambda_{3(L+1)^2-2}$ is the space spanned by all eigenfields of (62) with associated eigenvalue $\lambda = 0$. Fields $\mathbf{h}(\hat{\mathbf{r}})$ vanishing in $\Omega \setminus R$ without power in the spectral interval $0 \leq l \leq L$ are members of this null space.

3.3. Significant and insignificant eigenvalues

The eigenvalues of the matrix \mathbf{K} defined in (39) can be summed up as follows

$$\begin{aligned} N &= \sum_{\alpha=1}^{3(L+1)^2-2} \lambda_\alpha = \text{tr } \mathbf{K} = \sum_{lm}^L (P_{lm,lm} + B_{lm,lm} + C_{lm,lm}) \\ &= \int_R \left[\sum_{lm}^L \mathbf{P}_{lm}(\hat{\mathbf{r}}) \cdot \mathbf{P}_{lm}(\hat{\mathbf{r}}) + \mathbf{B}_{lm}(\hat{\mathbf{r}}) \cdot \mathbf{B}_{lm}(\hat{\mathbf{r}}) + \mathbf{C}_{lm}(\hat{\mathbf{r}}) \cdot \mathbf{C}_{lm}(\hat{\mathbf{r}}) \right] d\Omega \\ &= [3(L+1)^2 - 2] \frac{A}{4\pi}. \end{aligned} \tag{65}$$

In the fourth equality we substituted the diagonal matrix elements $P_{lm,lm}$, $B_{lm,lm}$ and $C_{lm,lm}$ from (34), (43)–(44), and in the last equality we used the addition theorem (21).

The value N in (65) is the vector spherical analogue of the Shannon number in the scalar Slepian concentration problems [6]. Well-concentrated eigenfields $\mathbf{g}_\alpha(\hat{\mathbf{r}})$ for the region R will have eigenvalues λ_α near unity, whereas poorly concentrated eigenfields will have eigenvalues λ_α close to zero. Due to the characteristic step-shaped spectrum of eigenvalues $\lambda_1, \lambda_2, \dots, \lambda_{3(L+1)^2-2}$, the total number of significant ($\lambda_\alpha \approx 1$) eigenvalues can be well approximated by the rounded sum (65), as in the one-dimensional and two-dimensional scalar spherical problems. Since N is a good estimate for the number of significant eigenvalues, then, roughly speaking, the vector spherical Shannon number (65) describes the dimension of the space of vector fields $\mathbf{u}(\hat{\mathbf{r}})$ that are approximately limited in both the spectral domain to vector spherical-harmonic degrees $0 \leq l \leq L$, and in the spatial domain to an arbitrarily shaped region R of area A [62,63].

Instead of constructing a bandlimited field $\mathbf{g}(\hat{\mathbf{r}}) \in \mathcal{S}_L$ that is optimally energy-concentrated within a spatial region R , we could have sought to construct one that is optimally excluded from R , i.e., one that is optimally concentrated within $\Omega \setminus R$, and therefore sought to minimize rather than maximize the Rayleigh quotient (31). What we have constructed are the stationary solutions $\mathbf{g}(\hat{\mathbf{r}}) \in \mathcal{S}_L$ of (31). Therefore we have actually solved the concentration and exclusion problems simultaneously. The optimally excluded eigenfields are identical to the optimally concentrated eigenfields but with reversed ordering. Because λ_α is the fractional power of \mathbf{g}_α within R , its fractional power within $\Omega \setminus R$ is $1 - \lambda_\alpha$. If the region R of area A covers only a small fraction of the sphere $A \ll 4\pi$, the number of well-excluded eigenfields will be much larger than the number of well-concentrated eigenfields.

We can express the kernel $\mathbf{K}(\hat{\mathbf{r}}, \hat{\mathbf{r}}')$ in the integral eigenvalue equation (56) in terms of the spatial-domain eigenfields $\mathbf{g}_1, \mathbf{g}_2, \dots, \mathbf{g}_{3(L+1)^2-2}$ in the form

$$\mathbf{K}(\hat{\mathbf{r}}, \hat{\mathbf{r}}') = \sum_{\alpha=1}^{3(L+1)^2-2} \mathbf{g}_\alpha(\hat{\mathbf{r}}) \mathbf{g}_\alpha(\hat{\mathbf{r}}'). \tag{66}$$

Eq. (66) is equivalent to the original representation (57), because both the $\mathbf{P}_{lm}, \mathbf{B}_{lm}, \mathbf{C}_{lm}$, $0 \leq l \leq L$, $-l \leq m \leq l$, and the \mathbf{g}_α , $\alpha = 1, 2, \dots, 3(L+1)^2 - 2$, are $[3(L+1)^2 - 2]$ -dimensional orthonormal bases for \mathcal{S}_L , and the transformation matrix that consists of the eigenvectors is orthogonal. The transformed representation (66) is a vector-spherical version of Mercer's

theorem [61,64,65]. Upon setting $\hat{\mathbf{r}}' = \hat{\mathbf{r}}$ in (66) and applying the trace [52], we deduce that the sum of the squares of the $3(L + 1)^2 - 2$ bandlimited eigenfields $\mathbf{g}_\alpha(\hat{\mathbf{r}})$ is a constant that is independent of position $\hat{\mathbf{r}}$ on the sphere Ω ,

$$\sum_{\alpha=1}^{3(L+1)^2-2} \mathbf{g}_\alpha(\hat{\mathbf{r}}) \cdot \mathbf{g}_\alpha(\hat{\mathbf{r}}) = \frac{3(L+1)^2-2}{4\pi} = \frac{N}{A}. \tag{67}$$

If the eigenvalues of the first N eigenfields $\mathbf{g}_1(\hat{\mathbf{r}}), \mathbf{g}_2(\hat{\mathbf{r}}), \dots, \mathbf{g}_N(\hat{\mathbf{r}})$ are near unity, and the remaining eigenvalues $\mathbf{g}_{N+1}(\hat{\mathbf{r}}), \mathbf{g}_{N+2}(\hat{\mathbf{r}}), \dots, \mathbf{g}_{3(L+1)^2-2}(\hat{\mathbf{r}})$ are near zero, then we expect the eigenvalue-weighted sum of squares to be

$$\sum_{\alpha=1}^{3(L+1)^2-2} \lambda_\alpha \mathbf{g}_\alpha(\hat{\mathbf{r}}) \cdot \mathbf{g}_\alpha(\hat{\mathbf{r}}) \approx \sum_{\alpha=1}^N \lambda_\alpha \mathbf{g}_\alpha(\hat{\mathbf{r}}) \cdot \mathbf{g}_\alpha(\hat{\mathbf{r}}) \approx \begin{cases} N/A & \text{if } \hat{\mathbf{r}} \in R, \\ 0 & \text{otherwise.} \end{cases} \tag{68}$$

The terms with $N + 1 \leq \alpha \leq 3(L + 1)^2 - 2$ should be comparatively small. It is hence immaterial whether we include them in the sum (68) or not. The combination of the first N orthogonal eigenfields $\mathbf{g}_\alpha, \alpha = 1, 2, \dots, N$, with eigenvalues $\lambda_\alpha \approx 1$, provides an essentially uniform coverage of the region R . This characterizes the spatio-spectral concentration problem: the spatio-spectrally concentrated basis effectively reduces the number of degrees of freedom from $\dim S_L = 3(L + 1)^2 - 2$ to $N = \lceil 3(L + 1)^2 - 2 \rceil A / (4\pi)$.

3.4. Pairs of spatially concentrated tangential vector fields

It is possible to construct, from one spatially concentrated, bandlimited tangential vector field another orthogonal, equally concentrated and equally bandlimited vector field, by simply rotating its vectorial directions at each point on the sphere by 90° while retaining the absolute values. Such pairs of tangential Slepian fields already appear in the purely tangential eigenvalue problem, which, due to the block-diagonal shape of \mathbf{K} in (39), can be solved independently from the radial problem (37). From (46) we obtain the purely tangential concentration problem

$$\mathbf{Q}\mathbf{g} = \begin{pmatrix} \mathbf{B} & \mathbf{D} \\ -\mathbf{D} & \mathbf{B} \end{pmatrix} \mathbf{g} = \lambda \mathbf{g}. \tag{69}$$

If $\mathbf{g} = (g_1, g_2)^T$ is an eigenvector of (69) with eigenvalue λ , then $\mathbf{g} = (-g_2, g_1)^T$ is also an eigenvector with the same associated eigenvalue λ . The Slepian field constructed from $(-g_2, g_1)^T$ has the same pointwise absolute value as the Slepian field constructed from $(g_1, g_2)^T$, and they are pointwise orthogonal.

4. Concentration within an axisymmetric polar cap

In this section we concentrate on the special but important case where R is a symmetric polar cap with colatitudinal radius Θ , that is centered on the north pole, as is shown in Fig. 1. Because rotations on the sphere commute with the operators (16)–(18) that define the vector spherical harmonics [58], the optimally concentrated eigenfields of the polar cap $R = \{\theta: 0 \leq \theta \leq \Theta\}$ can be rotated to anywhere on the unit sphere using the same transformations that apply in the rotation of scalar functions [52,54,66].

4.1. Decomposition of the spectral-domain eigenvalue problem

In the axisymmetric case the matrix elements (34) and (43)–(45) reduce to

$$P_{lm,l'm'} = 2\pi \delta_{mm'} \int_0^\Theta X_{lm} X_{l'm} \sin \theta \, d\theta, \tag{70}$$

$$B_{lm,l'm'} = \frac{2\pi \delta_{mm'} \int_0^\Theta [X'_{lm} X'_{l'm} + m^2 (\sin \theta)^{-2} X_{lm} X_{l'm}] \sin \theta \, d\theta}{\sqrt{l(l+1)l'(l'+1)}}, \tag{71}$$

$$D_{lm,l'm'} = -\frac{2\pi \delta_{-mm'} m X_{lm}(\Theta) X_{l'm}(\Theta)}{\sqrt{l(l+1)l'(l'+1)}}, \tag{72}$$

while, as we know from (46) also, $C_{lm,l'm'} = B_{lm,l'm'}$, and we remember (6).

The Kronecker deltas $\delta_{mm'}$ and $\delta_{-mm'}$ admit rearranging the $(L + 1)^2 \times (L + 1)^2$ radial-component matrix \mathbf{P} and the $[2(L + 1)^2 - 2] \times [2(L + 1)^2 - 2]$ tangential-component matrix \mathbf{Q} such that both of these are block-diagonal: $\mathbf{P} = \text{diag}(\mathbf{P}_0, \mathbf{P}_1, \mathbf{P}_{-1}, \dots, \mathbf{P}_L, \mathbf{P}_{-L})$ and $\mathbf{Q} = \text{diag}(\mathbf{Q}_0, \mathbf{Q}_1, \mathbf{Q}_{-1}, \dots, \mathbf{Q}_L, \mathbf{Q}_{-L})$.

Instead of solving the full eigenvalue equation (47), we can thus elect to solve a series of smaller spectral-domain algebraic eigenvalue problems, one for each order,

$$P_m g = \lambda g \quad \text{and} \quad Q_m g = \lambda g. \tag{73}$$

The matrices P_m and Q_m are of the form

$$P_m = \begin{pmatrix} P_{mm}^m & \cdots & P_{mL}^m \\ \vdots & & \vdots \\ P_{Lm}^m & \cdots & P_{LL}^m \end{pmatrix}, \quad Q_m = \begin{pmatrix} B_m & D_m \\ D_m^T & B_m \end{pmatrix}, \tag{74}$$

with

$$B_m = \begin{pmatrix} B_{mm}^m & \cdots & B_{mL}^m \\ \vdots & & \vdots \\ B_{Lm}^m & \cdots & B_{LL}^m \end{pmatrix}, \quad D_m = \begin{pmatrix} D_{mm}^m & \cdots & D_{mL}^m \\ \vdots & & \vdots \\ D_{Lm}^m & \cdots & D_{LL}^m \end{pmatrix}, \tag{75}$$

where, for any particular harmonic order $0 \leq m \leq L$ and degree $m \leq l, l' \leq L$, we denote $P_{ll'}^m = P_{lm, l'm}$, and, likewise, for $\max(m, 1) \leq l, l' \leq L$, we denote $B_{ll'}^m = B_{lm, l'm}$, and $D_{ll'}^m = D_{lm, l' - m}$. We then also have

$$P_{-m} = P_m, \quad B_{-m} = B_m, \quad D_{-m} = -D_m, \quad D_0 = 0, \tag{76}$$

and that P_m, B_m, D_m , and consequently, Q_m , are symmetric.

The calculations of the matrix elements $D_{ll'}^m$ are straightforward since they merely consist in evaluating the X_{lm} at θ . The calculations of the product integrals $P_{ll'}^m$ and $B_{ll'}^m$ can be simplified to integrations over individual terms X_{lm} . For example, for the elements $P_{ll'}^m$ we can directly apply (5) to reduce them to

$$P_{ll'}^m = \sqrt{\pi(2l+1)(2l'+1)} \sum_{n=|l-l'|}^{l+l'} \sqrt{2n+1} \begin{pmatrix} l & n & l' \\ 0 & 0 & 0 \end{pmatrix} \begin{pmatrix} l & n & l' \\ m & -2m & m \end{pmatrix} \int_0^\theta X_{n2m}(\theta) \sin \theta \, d\theta, \tag{77}$$

and those can be handled recursively via Eqs. (11) to (13). Here, as before, we set $X_{lm} = 0$ for $m > l$. Since this solution to (37) is identical to that of the scalar spherical concentration problem for the polar cap, alternate expressions and special cases can be found elsewhere [7,67]. For the $B_{ll'}^m$ at positive orders $m \geq 0$, as first noted by Eshagh [37], we first need to transform the derivative products $X'_{lm} X'_{l'm}$, and $m^2(\sin \theta)^{-2} X_{lm} X'_{l'm}$, into products of X_{lm} using the lemmas (7)–(10), to

$$\begin{aligned} \int_0^\theta X'_{lm} X'_{l'm} \sin \theta \, d\theta &= a_{lm}^- a_{l'm}^- \int_0^\theta X_{l_{m-1}} X_{l'_{m-1}} \sin \theta \, d\theta + a_{lm}^+ a_{l'm}^- \int_0^\theta X_{l_{m+1}} X_{l'_{m-1}} \sin \theta \, d\theta \\ &\quad + a_{lm}^- a_{l'm}^+ \int_0^\theta X_{l_{m-1}} X_{l'_{m+1}} \sin \theta \, d\theta + a_{lm}^+ a_{l'm}^+ \int_0^\theta X_{l_{m+1}} X_{l'_{m+1}} \sin \theta \, d\theta, \end{aligned} \tag{78}$$

$$\begin{aligned} &\int_0^\theta m^2(\sin \theta)^{-2} X_{lm} X'_{l'm} \sin \theta \, d\theta \\ &= b_{lm}^- b_{l'm}^- \int_0^\theta X_{l_{-1m-1}} X_{l'_{-1m-1}} \sin \theta \, d\theta + b_{lm}^+ b_{l'm}^- \int_0^\theta X_{l_{-1m+1}} X_{l'_{-1m-1}} \sin \theta \, d\theta \\ &\quad + b_{lm}^- b_{l'm}^+ \int_0^\theta X_{l_{-1m-1}} X_{l'_{-1m+1}} \sin \theta \, d\theta + b_{lm}^+ b_{l'm}^+ \int_0^\theta X_{l_{-1m+1}} X_{l'_{-1m+1}} \sin \theta \, d\theta, \end{aligned} \tag{79}$$

where a_{lm}^\pm and b_{lm}^\pm are defined in (8) and (10). The right hand sides of (78) and (79) can be expanded using (5) and then the recursion (11) to (13) can be applied.

We order the $L - m + 1$ distinct eigenvalues of P_m and the $2[L - \max(m, 1) + 1]$ distinct eigenvalues of Q_m obtained by solving each of the eigenvalue problems (73) so that $1 \geq \lambda_1 \geq \lambda_2 \geq \dots > 0$. Additionally we orthonormalize the associated eigenvectors g_1, g_2, \dots as in (48) so that

$$g_\alpha^T g_\beta = \delta_{\alpha\beta}, \quad g_\alpha^T P_m g_\beta = \lambda_\alpha \delta_{\alpha\beta} \quad \text{or} \quad g_\alpha^T Q_m g_\beta = \lambda_\alpha \delta_{\alpha\beta}, \tag{80}$$

depending on whether g_α and g_β are the eigenvectors of P_m or of Q_m .

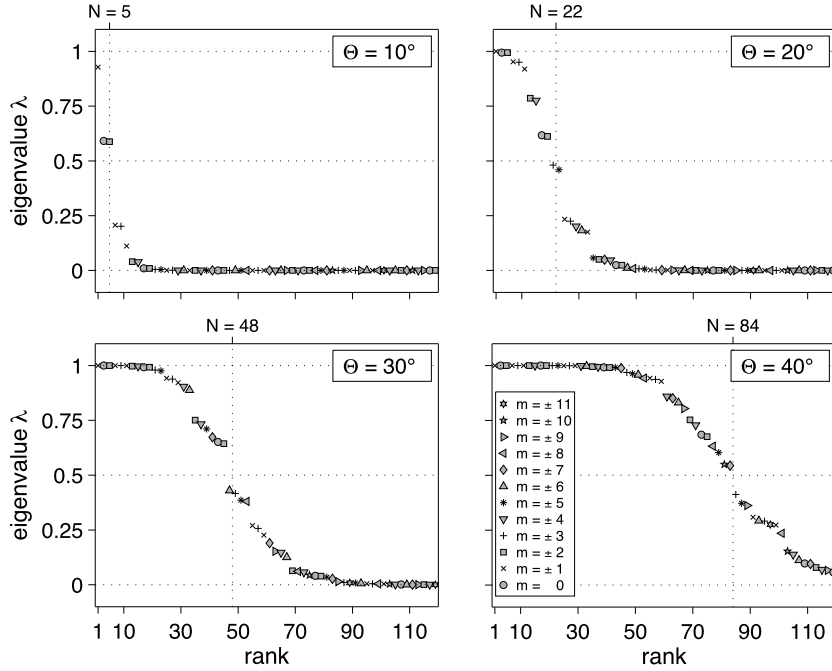


Fig. 2. Reordered eigenvalue spectra (λ_α versus rank α) for the tangential vector Slepian functions for axisymmetric polar caps of colatitudinal radii $\Theta = 10^\circ, 20^\circ, 30^\circ, 40^\circ$ and a common bandwidth $L = 18$. The total number of eigenvalues is $2(L+1)^2 - 2 = 720$; only λ_1 through λ_{120} are shown. Different symbols are used to plot the orders $-11 \leq m \leq 11$. Each symbol stands for two eigenvalues, that is, the $\pm m$ doublets for $m > 0$ and the doublets stemming from the block-diagonal shape of Q_0 for $m = 0$. Vertical gridlines and top labels specify the rounded Shannon numbers $N^t = 5, 22, 48$, and 84 .

4.2. Eigenvalue spectrum and eigenfields

For the fixed-order radial eigenvalue problem (73) we can calculate the number of significant eigenvalues, or partial Shannon number, using any of the two formulas

$$N_m^r = \sum_{\alpha=1}^{L-m+1} \lambda_\alpha = \sum_{l=m}^L P_{ll}^m. \quad (81)$$

For the fixed-order tangential eigenvalue problem (73) we obtain the number of significant eigenvalues from

$$N_m^t = \sum_{\alpha=1}^{2[L-\max(m,1)+1]} \lambda_\alpha = 2 \sum_{l=\max(m,1)}^L B_{ll}^m. \quad (82)$$

Once we have found the $L+1$ sequences of fixed-order radial and tangential eigenvalues, we can re-sort them into an overall mixed-order ranking. The Shannon number of radial eigenvalues is then given by $N^r = N_0^r + 2 \sum_{m=1}^L N_m^r$, while that of the tangential eigenvalues is $N^t = N_0^t + 2 \sum_{m=1}^L N_m$. The factor of two accounts for the $\pm m$ degeneracy; the total number of significantly concentrated vector fields is $N = N^r + N^t$.

Fig. 2 shows the reordered, mixed- m eigenvalue spectra calculated for four different polar caps, with colatitudinal radii $\Theta = 10^\circ, 20^\circ, 30^\circ, 40^\circ$, for the case of the tangential concentration problem. The spherical-harmonic bandlimit is $L = 18$. Each symbol stands for two eigenvalues, arising from the plus-minus-degeneracy for $m > 0$ and from the block-diagonal shape for $m = 0$. The spectra have a characteristic step shape [62,68,69], showing significant ($\lambda \approx 1$) and insignificant ($\lambda \approx 0$) eigenvalues separated by a transition band. In all four cases the reasonably well-concentrated eigensolutions ($\lambda \geq 0.5$) and the more poorly concentrated ones ($\lambda < 0.5$) are separated by the rounded Shannon number.

Fig. 3 shows a polar plot of the absolute values of the first 32 tangential eigenfields $|\mathbf{g}(\hat{\mathbf{r}})|$ constructed from the eigenvectors of Q . The reconstructed fields for positive and negative orders $\pm m$ have the same absolute values. We therefore only plot the absolute values for $m \geq 0$. The eigenfields are concentrated within a cap of radius $\Theta = 40^\circ$. The maximal vector spherical-harmonic degree is $L = 18$ and the Shannon number of the tangential problem $N^t = 84$. The eigenvalue ranking is mixed-order and the concentration factors $1 < \lambda \leq 0.937$ and orders m of each absolute field are indicated. Red (in the web version of this article) denotes the maximum value while all absolute values smaller than 1% of the maximum value are white.

In Fig. 4 we illustrate the best-concentrated tangential Slepian fields for order $|m| = 1$, corresponding to the overall best-concentrated absolute field of Fig. 3. The left panel shows the vector field for $m = 1$, thus the reconstruction using the

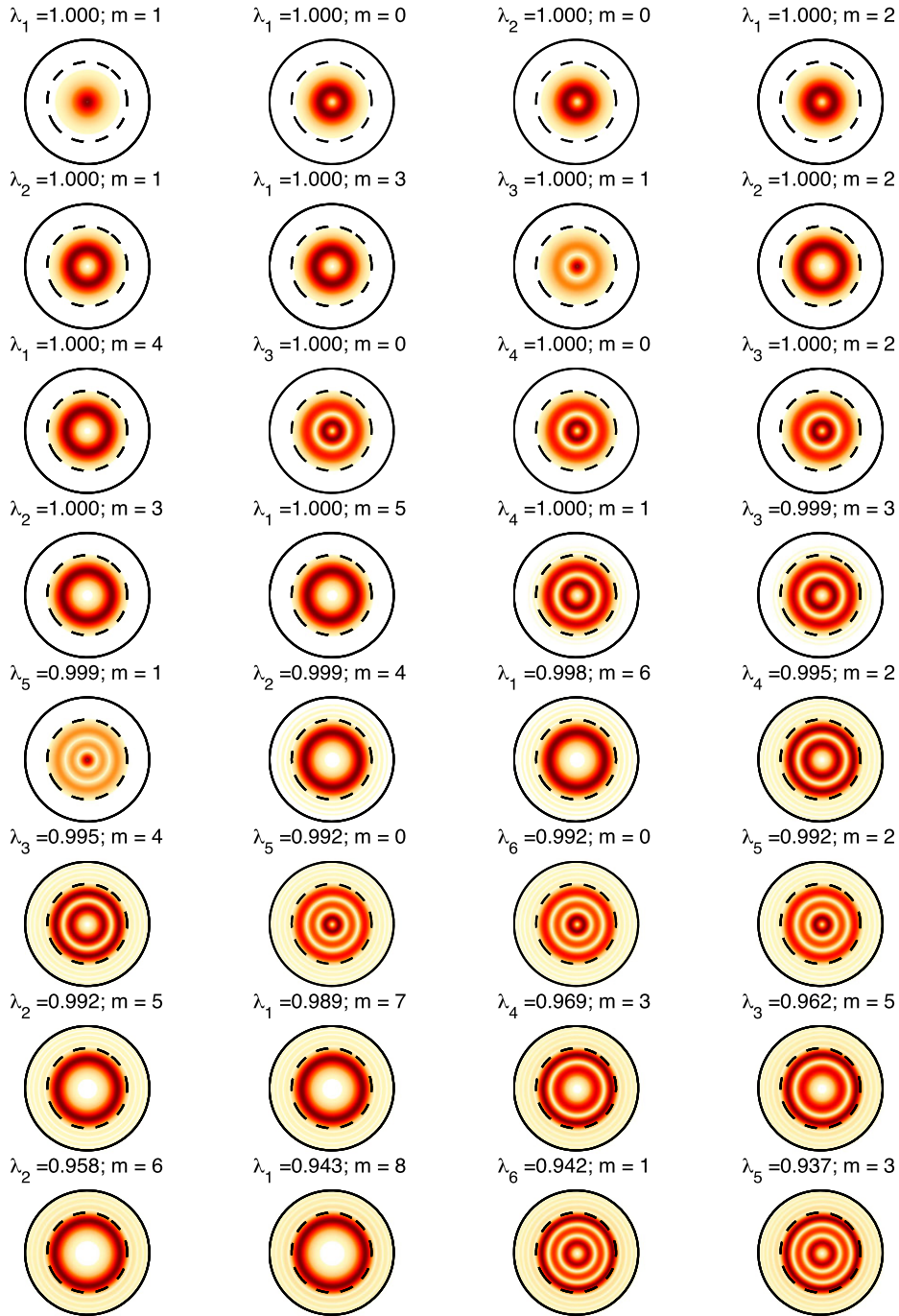


Fig. 3. Absolute values of the tangential bandlimited eigenfields, $|g(\theta, \phi)|$, that are optimally concentrated within a circular cap of colatitudinal radius $\Theta = 40^\circ$. Dashed circles denote the cap boundary. The bandwidth is $L = 18$, and the rounded Shannon number for the tangential space $N^t = 84$. Subscripts on the eigenvalues λ_α specify the fixed-order rank. Only absolute values for $m \geq 0$ are shown because the absolute values for $\pm m$ are identical. The eigenvalues have been re-sorted into a mixed-order ranking, with the best-concentrated eigenfields plotted on the top left and a decreasing concentration ratio to the right and downwards. Regions in which the absolute value is less than one hundredth of the maximum value on the sphere are left white.

best-concentrated eigenvector of Q_1 . The right panel shows the vector field for $m = -1$, thus the reconstruction using the best-concentrated eigenvector of Q_{-1} . As in Fig. 3, the radius of the polar cap is $\Theta = 40^\circ$ and the bandwidth $L = 18$. Both vector fields have a singularity at the north pole $\theta = 0$. This is due to the fact that all the \mathbf{B}_{lm} and \mathbf{C}_{lm} for $m = 1$ have a singularity at the north pole stemming from the derivatives of the X_{lm} (7) which are not equal to zero at $\theta = 0$. The dashed circles denote the cap boundary. The color scales with the absolute value of the vector field, ranging from white for values

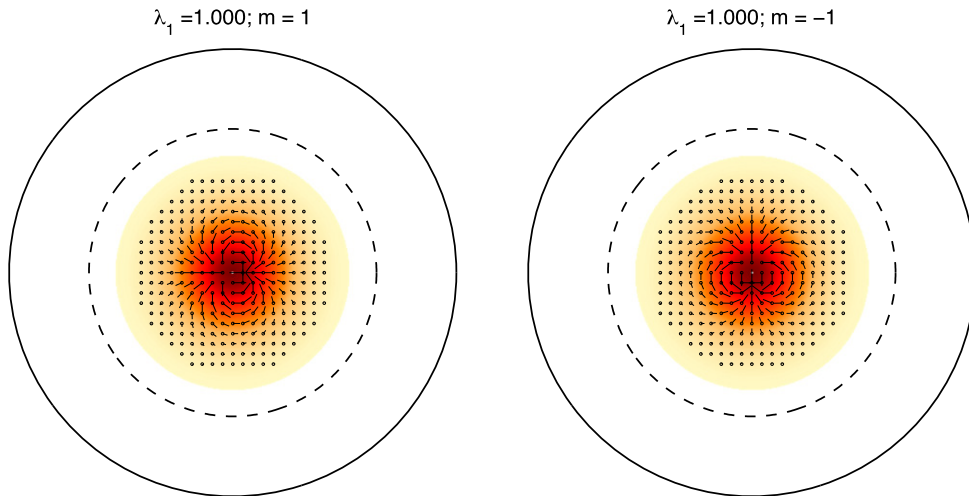


Fig. 4. Bandlimited tangential Slepian functions, $\mathbf{g}(\theta, \phi)$, of spherical-harmonic orders $m = \pm 1$, optimally concentrated within a polar cap of radius $\Theta = 40^\circ$. The bandwidth is $L = 18$. Color is absolute value (red the maximum) and circles with strokes indicate the direction of the eigenfield on the tangential plane. Regions in which the absolute value is less than one hundredth of the maximum absolute value on the sphere are left white. (For interpretation of the references to color in this figure legend, the reader is referred to the web version of this article.)

Table 1

Fractional areas, tangential Shannon numbers, and bandwidths for the vectorial concentration problem to continental areas.

| Continental region | Fractional area $A/(4\pi)$ (%) | Tangential Shannon number N^t | | | |
|--------------------|-----------------------------------|---------------------------------|----------|----------|----------|
| | | $L = 6$ | $L = 12$ | $L = 18$ | $L = 24$ |
| Greenland | 0.43 | 0 | 1 | 3 | 5 |
| Australia | 1.51 | 1 | 5 | 11 | 19 |
| Antarctica | 2.72 | 3 | 9 | 20 | 34 |
| South America | 3.45 | 3 | 12 | 25 | 43 |
| North America | 4.03 | 4 | 14 | 29 | 50 |
| Africa | 5.81 | 6 | 20 | 42 | 73 |
| Eurasia | 9.97 | 10 | 33 | 72 | 124 |

below 1% of the maximum to red (in the web version of this article) for the maximum value. The directions of the field are indicated by accordingly oriented strokes at the positions marked by the open circles.

5. Continental concentration

In the following example we consider the spatio-spectral concentration in seven of Earth's continental regions. Together with their rounded tangential-component Shannon numbers, $N^t = [2(L+1)^2 - 2]A/(4\pi)$, the regions are listed in Table 1 for different bandwidths. The (tangential) spherical Slepian fields that we will be showing should be well suited to the localized analysis of global vector-valued satellite-magnetic data such as measured to study the magnetization of the terrestrial lithosphere (e.g. [40,70–72]), or more generally, planetary magnetic fields [18,73–75].

5.1. Bandlimited fields

Fig. 5 shows the eigenvalue spectra of the tangential Slepian fields for the five regions Greenland, Australia, North America, Africa, and Eurasia, and four spherical-harmonic bandlimits, $L = 6, 12, 18, 24$, which correspond to $2(L+1)^2 - 2 = 96, 336, 720, 1248$ eigenfields each. The smallest wavelength for a bandwidth limit L is $2\pi/\sqrt{L(L+1)} \approx 2\pi/(L+1/2)$ multiplied by Earth's radius [53]. The cutoff wavelengths for $L = 6, 12, 18$, and 24 are 6200, 3200, 2200, and 1600 km, respectively. Only Eurasia, the largest region, has enough area to contain at least one nearly perfectly concentrated eigenfield for the smallest bandwidth, $L = 6$, and Greenland, the smallest of the considered regions, is too small to contain even for the largest bandwidth, $L = 24$, a single eigenfield with a concentration factor λ near unity. Again, as was the case for a polar cap (Fig. 2), the well-concentrated eigenfunctions with eigenvalues $\lambda \geq 0.5$ are separated from the poorly concentrated ones with eigenvalues $\lambda < 0.5$ by the rounded Shannon numbers N^t . The eigenvalues occur in pairs as described in Section 3.4.

Figs. 6–7 are map views of the twelve best-concentrated tangential eigenfields $\mathbf{g}_1(\hat{\mathbf{r}}), \mathbf{g}_2(\hat{\mathbf{r}}), \dots, \mathbf{g}_{12}(\hat{\mathbf{r}})$ for the continents Africa and Antarctica, at $L = 18$. In either case, pairs of eigenfields have identical absolute values and the same associated eigenvalues but show vectorial directions that are pointwise perpendicular, see Section 3.4. All eigenfields for Antarctica have a singularity or are zero at the south pole. This comes from the fact that all tangential vector spherical harmonics (17)–(18) either have a singularity or are zero at the south pole. Both figures show that the first 12 tangential eigenfields are well

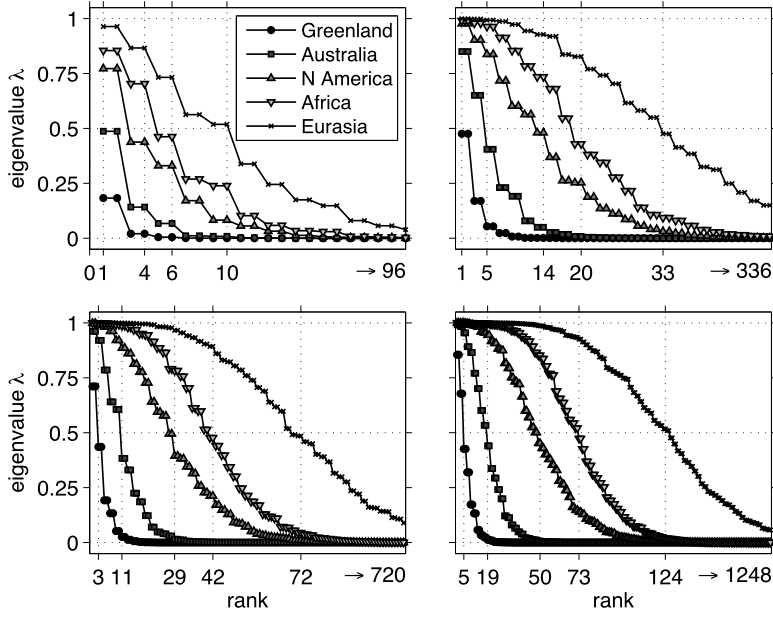


Fig. 5. Eigenvalue spectra for the tangential fields for Greenland, Australia, North America, Africa, and Eurasia. From upper left to lower right, four bandwidths, $L = 6, 12, 18, 24$, are considered. The horizontal axis in each panel is truncated; the total number of eigenvalues $2(L + 1)^2 - 2 = 96, 336, 720, 1248$, appears to the right of the arrow. Vertical gridlines and the five leftmost ordinate labels specify the rounded Shannon numbers N^l .

concentrated, which is also reflected by the tangential Shannon numbers, $N^l = 42$ for Africa and $N^l = 20$ for Antarctica. In both cases, the absolute values of the first two eigenfields are roughly circular domes centered in the middle of each continent. Subsequent orthogonal eigenfields $\mathbf{g}_3, \mathbf{g}_4, \dots$ exhibit lobes in previously uncovered regions. In Fig. 6, West Africa begins to be reasonably well covered by \mathbf{g}_5 and \mathbf{g}_6 , while Southern Africa is uncovered until \mathbf{g}_7 and \mathbf{g}_8 . Later, increasingly more oscillatory eigenfields cover smaller geographical features. For Antarctica, the third and fourth eigenfields \mathbf{g}_3 and \mathbf{g}_4 begin to resolve the South America-facing (western) and the Australia-facing (eastern) part of Antarctica, while the fifth and the sixth eigenfields \mathbf{g}_5 and \mathbf{g}_6 resolve the Africa-facing (northern) region and the region around the Transantarctic Mountains. Subsequent eigenfields show more nodal lines and resolve smaller geographical features.

Fig. 8 shows the eigenvalue-weighted sum of absolute squares $\sum_{\alpha} \lambda_{\alpha} |\mathbf{g}_{\alpha}(\hat{\mathbf{r}})|^2$ of the $L = 18$ bandlimited eigenfields of Earth's seven landmasses. The eigenfields $\mathbf{g}_1(\hat{\mathbf{r}}), \mathbf{g}_2(\hat{\mathbf{r}}), \dots, \mathbf{g}_{3(L+1)^2-2}(\hat{\mathbf{r}})$ can be found by diagonalizing the $[3(L + 1)^2 - 2] \times [3(L + 1)^2 - 2]$ matrix (39) formed by summing the matrices $\mathbf{K}_{\text{Eurasia}} + \mathbf{K}_{\text{Africa}} + \dots$ of each of the regions. The fractional area covered by all seven regions combined is $A/(4\pi) = 27.92\%$, and the corresponding rounded Shannon number $N = 302$; the figure shows the partial sums of the first $N/4, N/2$ and N terms, and the full sum of all $3(L + 1)^2 - 2 = 1081$ terms. It is apparent that the first N eigenfunctions uniformly cover the target region; by adding the remaining, poorly concentrated, $3(L + 1)^2 - 2 - N = 779$ terms, we only marginally improve the coverage. Because of its small size, Greenland does not appear until the $1 \rightarrow N/2$ partial sum. Even after the $1 \rightarrow N$ partial sum, Greenland's coverage is not perfect, as expected from its small Shannon number ($N = 5$ for $L = 18$).

5.2. Spacelimited fields

As described in Section 3.2, the spatially limited, spectrally concentrated vector fields $\mathbf{h}(\hat{\mathbf{r}})$ for a region R and bandlimit L can be calculated by either spacelimiting the spatially concentrated bandlimited fields for the same region R and the same bandlimit L , as expressed by (63), or by multiplying the coefficient vector \mathbf{g} of the spatially concentrated bandlimited field with a rectangular kernel matrix \mathbf{K} of infinite bandwidth in the first dimension.

Figs. 9 and 10 show such a construction for the combined six regions of Eurasia, Africa, North and South America, Australia, and Greenland, and a bandlimit of $L = 20$. Due to the block-diagonal shape of matrix \mathbf{K} in (39), the radial and tangential optimization problems are decoupled and were solved independently. The upper left panel of Fig. 9 shows the 80th best radial Slepian function $\mathbf{g}(\hat{\mathbf{r}})$, which by the measure (35) has 75.8% of its energy within the target region. Blue stands for inwards and red for outwards-pointing vectors. Areas with intensity of less than one percent of the maximum value are left white. The lower left panel of this figure shows the spherical-harmonic coefficients \mathbf{g} of this radial Slepian field. Shades of blue denote negative coefficient values and red positive values. Due to the bandlimitation, all coefficients with degree higher than $L = 20$ are zero. The upper right panel of Fig. 9 shows the spatially truncated radial Slepian field $\mathbf{h}(\hat{\mathbf{r}})$ and the lower right panel its spherical-harmonic coefficients \mathbf{h} . The coefficients U_{lm} are only shown up to $l = 40$ but

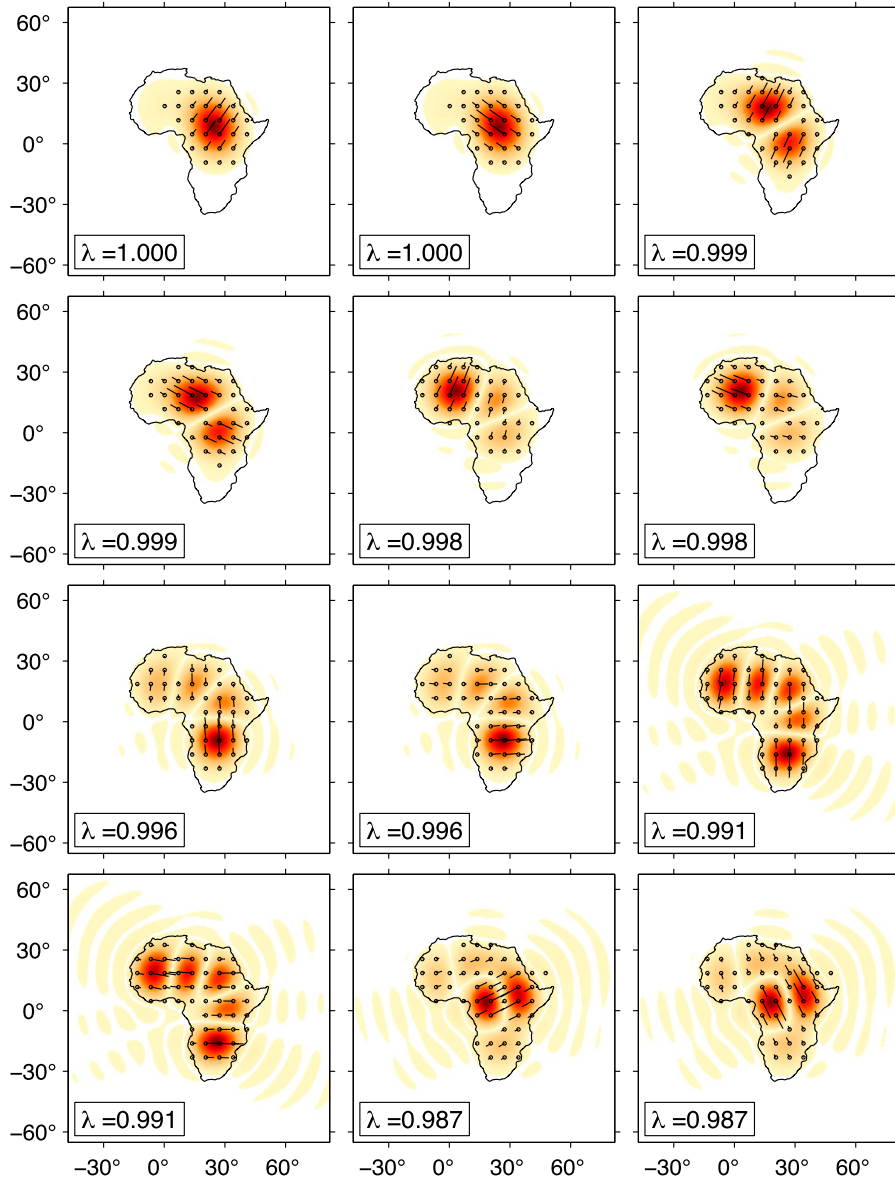


Fig. 6. Twelve tangential Slepian functions $\mathbf{g}_1, \mathbf{g}_2, \dots, \mathbf{g}_{12}$, bandlimited to $L = 18$, optimally concentrated within Africa. The concentration factors $\lambda_1, \lambda_2, \dots, \lambda_{12}$ are indicated. The rounded tangential Shannon number $N^t = 42$. Order of concentration is left to right, top to bottom. Color scheme and symbols are as in Fig. 4.

are non-zero to $l = \infty$ since $\mathbf{h}(\hat{\mathbf{r}})$ is perfectly spacelimited. The ratio (60), of the energy in the coefficients below $l = 20$ to the total energy, is once again 75.8%, illustrating the equivalence between the spatial and spectral concentration problems.

Fig. 10 illustrates the same procedure applied to tangential fields. The upper left panel shows the 160th best spatially concentrated bandlimited tangential field, with maximal spherical-harmonic degree $L = 20$. The middle left panel and the bottom left panel show the vector spherical-harmonic coefficients V_{lm} and W_{lm} , respectively. Again, the vector spherical-harmonic coefficients at degrees above the bandlimit $L = 20$ are zero. The right panels show the spacelimited and spectrally concentrated tangential vector Slepian field constructed from the bandlimited spatially concentrated vector Slepian field shown on the left, both in their spatial (uppermost panel) and spectral (middle and lower panels) renditions.

5.3. Constructive approximation

Finally, in order to demonstrate the spatial focusing capabilities of the bandlimited, spatially concentrated vector Slepian fields for an actual data example, we reconstruct a global tangential vector field, \mathbf{u} , by approximating it with fields \mathbf{v}_J that use an increasing number, J , of tangential vector Slepian functions:

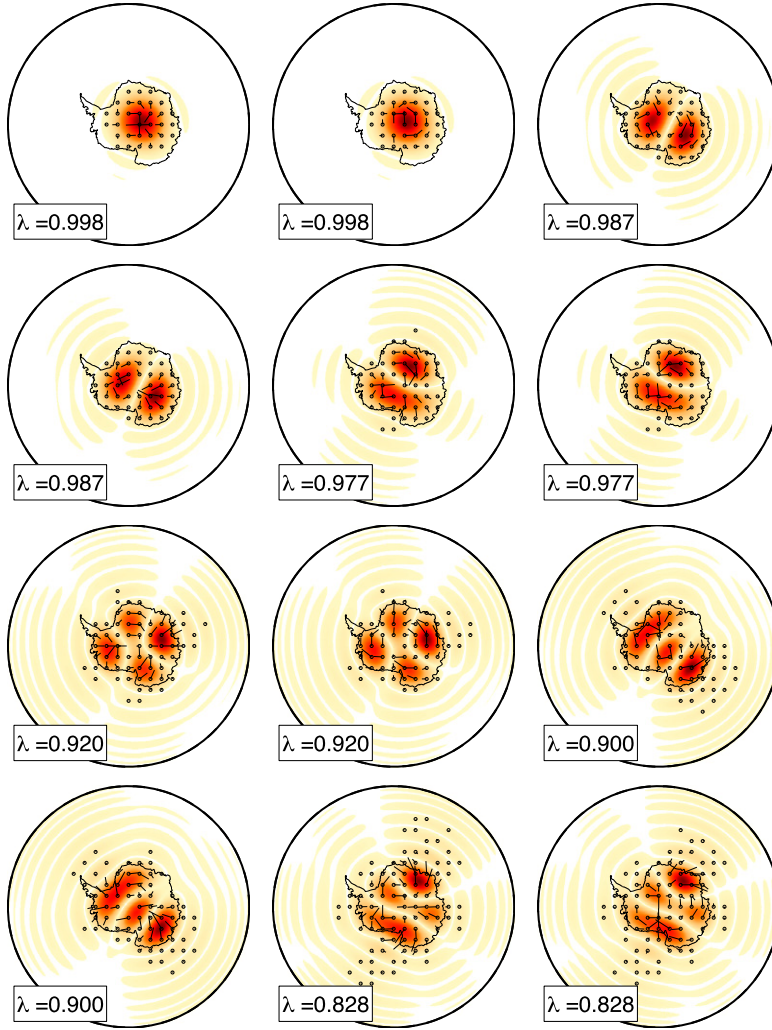


Fig. 7. Bandlimited $L = 18$ tangential eigenfields $\mathbf{g}_1, \mathbf{g}_2, \dots, \mathbf{g}_{12}$ that are optimally concentrated within Antarctica. The concentration factors $\lambda_1, \lambda_2, \dots, \lambda_{12}$ are indicated. The rounded tangential Shannon number is $N^t = 20$. Format is identical to that in Fig. 6.

$$\mathbf{v}_J = \sum_{\alpha=1}^J u_{\alpha} \mathbf{g}_{\alpha}. \tag{83}$$

The coefficients u_{α} are obtained by forming the inner product of the input field \mathbf{u} with the α best-concentrated vector Slepian functions \mathbf{g}_{α} . We define the relative error ϵ_J over the domain, and the leakage b_J to its complement, by

$$\epsilon_J = \sqrt{\frac{\|\mathbf{u} - \mathbf{v}_J\|_R^2}{\|\mathbf{u}\|_R^2}} \quad \text{and} \quad b_J = \sqrt{\frac{\|\mathbf{v}_J\|_{\Omega \setminus R}^2}{\|\mathbf{u}\|_{\Omega \setminus R}^2}}, \tag{84}$$

which we will use to assess the performance of the reconstruction. For bandlimited tangential fields \mathbf{u} the measure $\|\mathbf{u}\|_R^2$ can be calculated using the matrix \mathbf{Q} from (46) and the expansion coefficients $\mathbf{u} = (\dots, U_{lm}, \dots, V_{lm}, \dots, W_{lm}, \dots)^T$ by evaluating the expression $\|\mathbf{u}\|_R^2 = \mathbf{u}^T \mathbf{Q} \mathbf{u}$. The error decreases with increasing number of Slepian functions J . The bias increases with J . Our goal is to obtain a small reconstruction error within the region R while simultaneously keeping the outside leakage bias small.

Fig. 11 shows the outcome of such an experiment conducted on the terrestrial crustal-field model NGDC-720 V3 [76]. We multiply the spherical-harmonic coefficients with the corresponding \mathbf{B}_{lm} vector harmonics up to bandlimit $L = 72$. The left panel of Fig. 11 shows the tangential vector field that results: this is used as our input. The right panel shows the reconstruction using the $1.5N = 924$ best-concentrated tangential vector Slepian fields for Africa and the same bandlimit $L = 72$. While we chose $1.5N$ here for convenience, in real-world applications the optimal choice for the Slepian truncation would

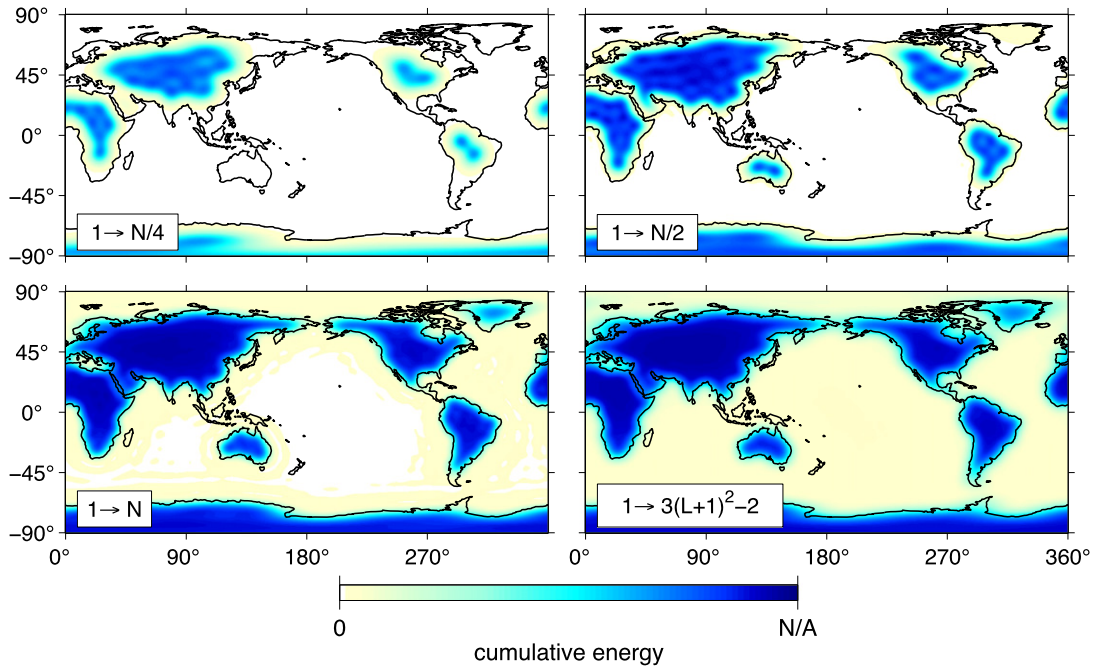


Fig. 8. Cumulative eigenvalue-weighted energy of the first $N/4$, $N/2$, N and all $3(L+1)^2 - 2$ eigenfields that are optimally concentrated within the ensemble of Eurasia, Africa, North America, South America, Antarctica, Australia, and Greenland. The bandwidth is $L = 18$; the cumulative fractional area $A/(4\pi) = 27.92\%$; the rounded Shannon number $N = 302$. The darkest blue on the color bar corresponds to the expected value (68) of the sum. Regions where the value is smaller than one hundredth of the N/A are left white. (For interpretation of the references to color in this figure legend, the reader is referred to the web version of this article.)

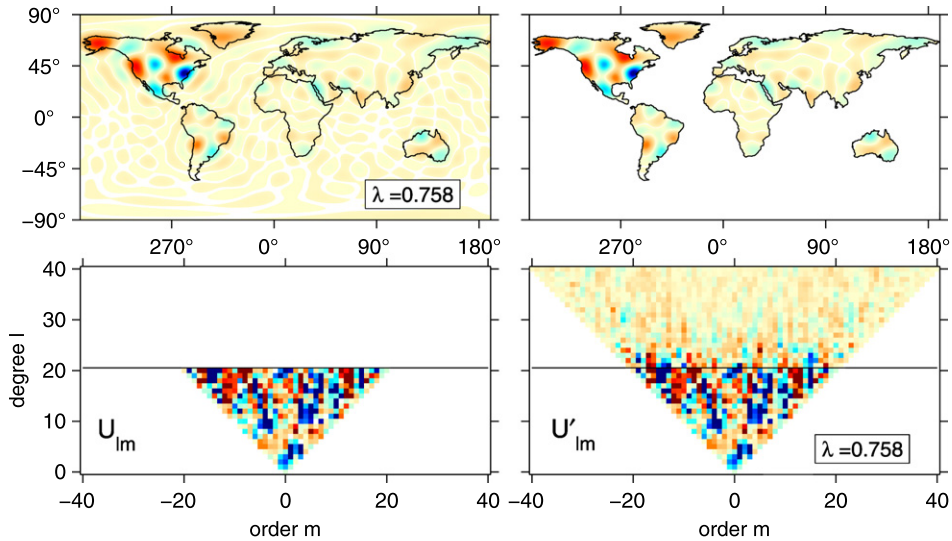


Fig. 9. The 80th best spatially concentrated bandlimited radial eigenfield (g_{80} , left panels) and the 80th best spectrally concentrated spacelimited eigenfield (h_{80} , right panels) for a spatial domain which is the ensemble of Eurasia, Africa, North America, South America, Australia and Greenland, and a bandwidth $L = 20$. The upper panels show the intensity and direction of the fields in the radial direction (blue inwards, red outwards). Regions where the absolute value is smaller than one hundredth of the maximum absolute value on the sphere are left white. The lower panels show the expansion coefficients for the radial vector harmonics P_{lm} of the fields shown in the panels above (blue negative, red positive).

depend on the behavior of the signal-to-noise ratio of the data [10,77,78]. The relative error and bias of the reconstruction over Africa, as defined by (84), are 0.4% and 14%, respectively.

Fig. 12 shows the evolution of error and bias for reconstructions using different numbers of Slepian-field terms in the expansion (83). The more Slepian fields are being used, the smaller the error over Africa, but the larger the leakage into the complimentary region outside of Africa. The relative reconstruction error over Africa drops quickly and reaches numerical noise level after $J = 1800$ Slepian function terms.

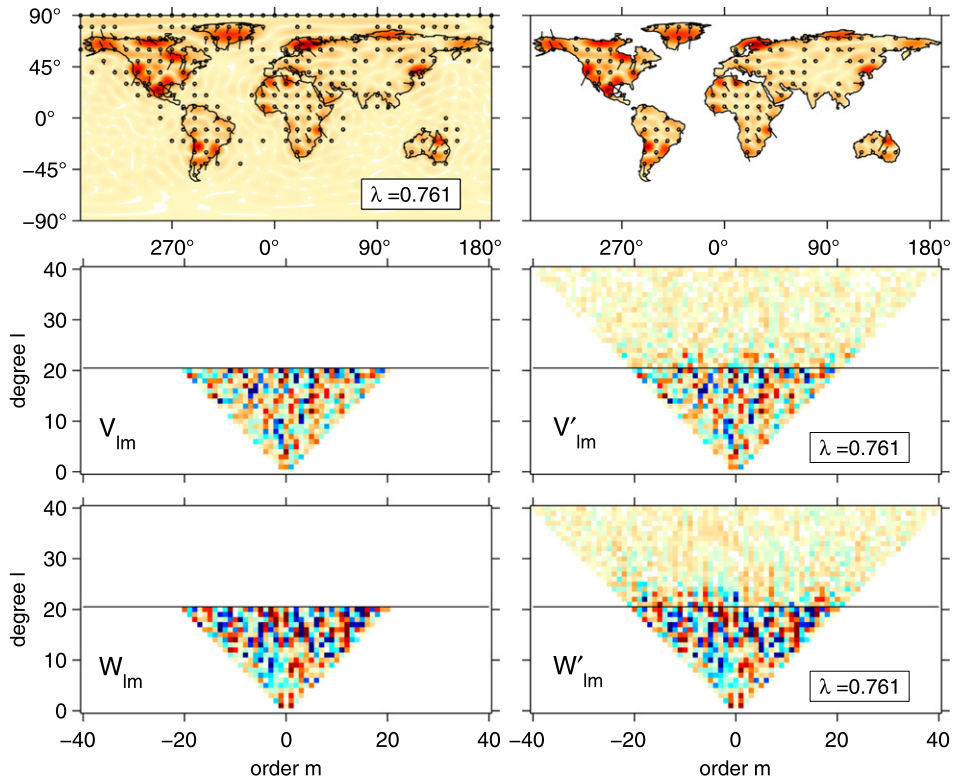


Fig. 10. The 160th best spatially concentrated bandlimited tangential eigenfield (\mathbf{g}_{160} , left panels) and the 160th best spectrally concentrated spacelimited eigenfield (\mathbf{h}_{160} , right panels) for a spatial domain which is the ensemble of Eurasia, Africa, North America, South America, Australia and Greenland, and a bandwidth $L = 20$. Uppermost panels show the intensity and direction of the fields. Regions where the absolute value is smaller than one hundredth of the maximum absolute value on the sphere are left white. Middle and lower panels show the expansion coefficients for the tangential vector harmonics \mathbf{B}_{lm} and \mathbf{C}_{lm} , respectively, of the fields shown in the uppermost panels (blue negative, red positive).

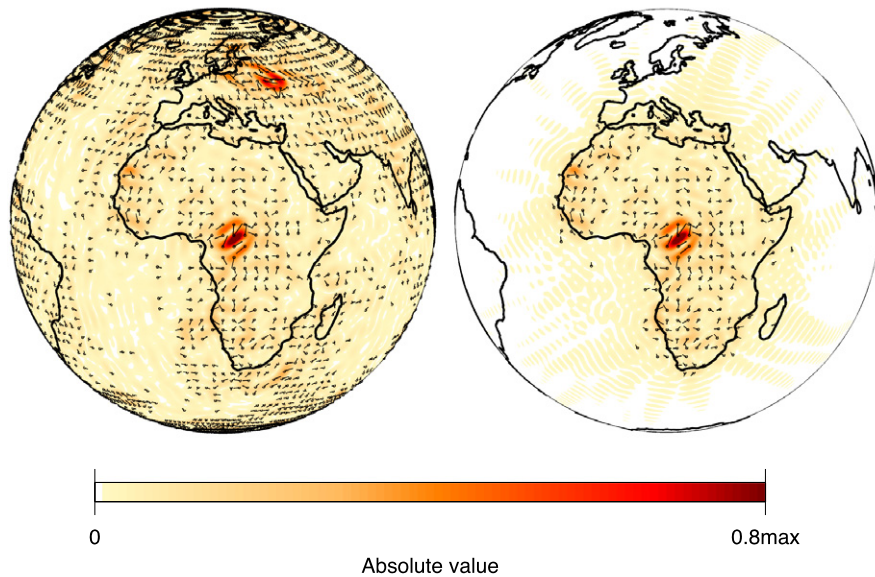


Fig. 11. A tangential geophysical vector field (left) and its reconstruction (right) using vectorial Slepian functions designed to maximize their spatial concentration over Africa. The bandlimit for both the original field and the Slepian basis is $L = 72$. There are 10,656 vectorial basis functions in the original field, and the same number of Slepian functions from which to choose for the reconstruction. The Shannon number $N^f = 620$. The bottom panel shows a reconstruction using the $924 = 1.5N^f$ best-concentrated Slepian functions for Africa. The error and bias over Africa, as defined in (84), are 0.4% and 14%, respectively.

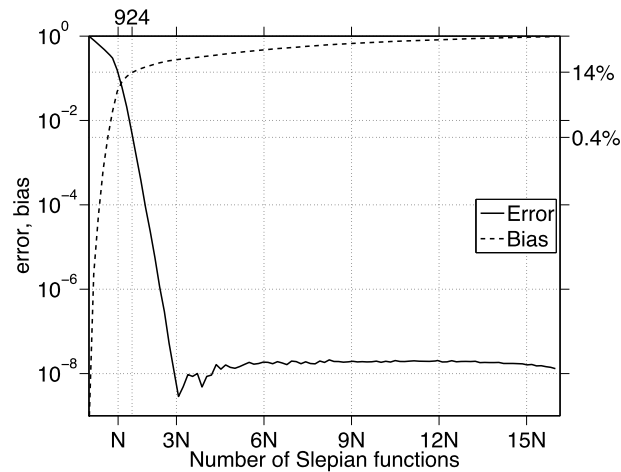


Fig. 12. Reconstruction error and bias over Africa as defined in (84), versus the number of vector Slepian functions used to describe the global vector field as shown in Fig. 11, quoted as a multiple of the Shannon number for this problem, $N^t = 620$.

6. Conclusion

It is possible to construct for the unit sphere a regionally optimally concentrated orthogonal family of bandlimited vector spherical-harmonic fields by solving either a Fredholm integral eigenvalue problem in the spatial domain, or, equivalently in the spectral domain, solving a symmetric finite-dimensional matrix eigenvalue problem. The eigenvalues $0 < \lambda < 1$ are measures of the spatial concentration of their corresponding bandlimited vector fields $\mathbf{g}(\hat{\mathbf{r}})$ and spectral concentration of the spacelimited eigenfields $\mathbf{h}(\hat{\mathbf{r}})$, which can be constructed from the $\mathbf{g}(\hat{\mathbf{r}})$ by setting the values to zero outside of the target region. The full vectorial problem decomposes into independent radial and tangential parts. The radial problem is equivalent to the scalar spherical spatio-spectral optimization problem [7]. The number of well-concentrated radial eigenfields is $N^r = (L + 1)^2 A / (4\pi)$ and the number of well-concentrated tangential eigenfields is $N^t = [2(L + 1)^2 - 2] A / (4\pi)$. Here L denotes the bandwidth and A the area of the target region. The Shannon numbers N^r and N^t can be interpreted as the dimensions of the spaces of radial vector fields $\mathbf{g}^r(\hat{\mathbf{r}})$, or tangential vector fields $\mathbf{g}^t(\hat{\mathbf{r}})$, respectively, that can be simultaneously concentrated within a subregion R of the sphere and within a spectral interval $0 \leq l \leq L$. In the special case of a circular polar cap, the kernel matrices can be computed analytically and decomposed into smaller eigenvalue problems.

Vectorial Slepian functions on the sphere are an emerging tool for the analysis and representation of essentially space- and bandlimited vector-valued functions on the surface of the unit sphere. In this contribution we have described their construction, shown various examples, and suggested their use in the constructive approximation of vectorial signals on the sphere, as may arise, for instance, in the fields of geophysics, planetary science, medical imaging and optics, where prior work has previously considered a number of special cases of the vectorial concentration on the sphere [26,79] that we have treated more completely here.

The ability of scalar Slepian functions on the sphere to perform localized bandlimited analysis has led to observations made from global data that remain obscured when applying global spherical harmonic analysis. For example, changes in local gravity after the 2004 Sumatra earthquake were detected [15,19] and shown to be invisible via a global spherical-harmonic analysis of the same data. Similarly, in analyzing global gravity data, the potential of scalar Slepian functions to detect local ice mass changes over Greenland was clearly demonstrated [17]. Judging from the equivalence in properties between the vectorial Slepian functions and the scalar Slepian functions in multiple Cartesian and spherical dimensions, it is likely that the impact of vectorial spherical Slepian functions on multidimensional vectorial signal processing will be as profound as the classical prolate spheroidal wave functions have been, and continue to be, in the study of time series, and this in a wide variety of scientific and engineering fields.

Acknowledgments

A.P. and F.J.S. thank Volker Michel for valuable discussions, and the Ulrich Schmucker Memorial Trust and the Swiss National Science Foundation for financial support. F.J.S. thanks Tony Dahlen (1942–2007) and Liying Wei for their contributions to the material developed in this manuscript. We thank the anonymous referee and the Editor-in-Chief Charles Chui. This work was partially supported by National Science Foundation grants EAR-1014606 and EAR-1150145 to F.J.S. To the historians of science we like to mention that we discovered reference [79] only after concluding our analysis, when completing our manuscript for submission.

References

- [1] D. Slepian, H.O. Pollak, Prolate spheroidal wave functions, Fourier analysis and uncertainty – I, *Bell Syst. Tech. J.* 40 (1) (1961) 43–63.
- [2] H.J. Landau, H.O. Pollak, Prolate spheroidal wave functions, Fourier analysis and uncertainty – II, *Bell Syst. Tech. J.* 40 (1) (1961) 65–84.
- [3] H.J. Landau, H.O. Pollak, Prolate spheroidal wave functions, Fourier analysis and uncertainty – III: The dimension of the space of essentially time- and band-limited signals, *Bell Syst. Tech. J.* 41 (4) (1962) 1295–1336.
- [4] D. Slepian, Some comments on Fourier analysis, uncertainty and modeling, *SIAM Rev.* 25 (3) (1983) 379–393.
- [5] D.J. Thomson, Spectrum estimation and harmonic analysis, *Proc. IEEE* 70 (1982) 1055–1096.
- [6] F.J. Simons, Slepian functions and their use in signal estimation and spectral analysis, in: W. Freedren, M.Z. Nashed, T. Sonar (Eds.), *Handbook of Geomathematics*, Chapter 30, Springer, Heidelberg, Germany, 2010, pp. 891–923, http://dx.doi.org/10.1007/978-3-642-01546-5_30.
- [7] F.J. Simons, F.A. Dahlen, M.A. Wieczorek, Spatiospectral concentration on a sphere, *SIAM Rev.* 48 (3) (2006) 504–536, <http://dx.doi.org/10.1137/S0036144504445765>.
- [8] F.J. Simons, D.V. Wang, Spatiospectral concentration in the Cartesian plane, *Internat. J. Geomath.* 2 (1) (2011) 1–36, <http://dx.doi.org/10.1007/s13137-011-0016-z>.
- [9] A. Albertella, F. Sacerdote, Using Slepian functions for local geodetic computations, *Boll. Geod. Sci. Affini* 60 (1) (2001) 1–14.
- [10] F.J. Simons, F.A. Dahlen, Spherical Slepian functions and the polar gap in geodesy, *Geophys. J. Int.* 166 (2006) 1039–1061, <http://dx.doi.org/10.1111/j.1365-246X.2006.03065.x>.
- [11] S.-C. Han, D.D. Rowlands, S.B. Luthcke, F.G. Lemoine, Localized analysis of satellite tracking data for studying time-variable Earth's gravity fields, *J. Geophys. Res.* 113 (2008) B06401, <http://dx.doi.org/10.1029/2007JB005218>.
- [12] D.C. Slobbe, F.J. Simons, R. Klees, The spherical Slepian basis as a means to obtain spectral consistency between mean sea level and the geoid, *J. Geod.* 86 (8) (2012) 609–628, <http://dx.doi.org/10.1007/s00190-012-0543-x>.
- [13] S.-C. Han, P. Ditmar, Localized spectral analysis of global satellite gravity fields for recovering time-variable mass redistributions, *J. Geod.* 82 (7) (2007) 423–430, <http://dx.doi.org/10.1007/s00190-007-0194-5>.
- [14] S.-C. Han, J. Sauber, S.B. Luthcke, C. Ji, F.F. Pollitz, Implications of postseismic gravity change following the great 2004 Sumatra–Andaman earthquake from the regional harmonic analysis of GRACE inter-satellite tracking data, *J. Geophys. Res.* 113 (2008) B11413, <http://dx.doi.org/10.1029/2008JB005705>.
- [15] S.-C. Han, F.J. Simons, Spatiospectral localization of global geopotential fields from the Gravity Recovery and Climate Experiment (GRACE) reveals the co-seismic gravity change owing to the 2004 Sumatra–Andaman earthquake, *J. Geophys. Res.* 113 (2008) B01405, <http://dx.doi.org/10.1029/2007JB004927>.
- [16] L. Longuevergne, B.R. Scanlon, C.R. Wilson, GRACE hydrological estimates for small basins: Evaluating processing approaches on the High Plains Aquifer, USA, *Water Resour. Res.* 46 (11) (2010) W11517, <http://dx.doi.org/10.1029/2009WR008564>.
- [17] C. Harig, F.J. Simons, Mapping Greenland's mass loss in space and time, *Proc. Natl. Acad. Sci.* 109 (49) (2012) 19934–19937, <http://dx.doi.org/10.1117/12.825730>.
- [18] J.-J. Schott, E. Thébault, Modelling the Earth's magnetic field from global to regional scales, in: M. Manda, M. Korte (Eds.), *Geomagnetic Observations and Models*, in: IAGA Spec. Sopron Book Ser., vol. 5, Springer, 2011, pp. 229–264.
- [19] F.J. Simons, J.C. Hawthorne, C.D. Beggan, Efficient analysis and representation of geophysical processes using localized spherical basis functions, in: V.K. Goyal, M. Papadakis, D. Van de Ville (Eds.), *Wavelets XIII*, in: Proc. SPIE, vol. 7446, SPIE, 2009, 74460G, <http://dx.doi.org/10.1117/12.825730>.
- [20] C. Harig, S. Zhong, F.J. Simons, Constraints on upper mantle viscosity inferred from the flow-induced pressure gradient across the Australian continental keel, *Geochem. Geophys. Geosyst.* 11 (6) (2010).
- [21] A.J. Evans, J.C. Andrews-Hanna, M.T. Zuber, Geophysical limitations on the erosion history within Arabia Terra, *J. Geophys. Res.* 115 (2010) E05007, <http://dx.doi.org/10.1029/2009JE003469>.
- [22] S. Goossens, Y. Ishihara, K. Matsumoto, S. Sasaki, Local lunar gravity field analysis over the South Pole-Aitken basin from SELENE farside tracking data, *J. Geophys. Res.* 117 (2012) E02005, <http://dx.doi.org/10.1029/2011JE003831>.
- [23] S.-C. Han, E. Mazarico, F.G. Lemoine, Improved nearside gravity field of the Moon by localizing the power law constraint, *Geophys. Res. Lett.* 36 (2009) L11203, <http://dx.doi.org/10.1029/2009GL038556>.
- [24] M.A. Wieczorek, Constraints on the composition of the Martian south polar cap from gravity and topography, *Icarus* 196 (2) (2008) 506–517, <http://dx.doi.org/10.1016/j.icarus.2007.10.026>.
- [25] H. Maniar, P.P. Mitra, The concentration problem for vector fields, *Int. J. Bioelectromagn.* 7 (1) (2005) 142–145.
- [26] P.P. Mitra, H. Maniar, Concentration maximization and local basis expansions (LBEX) for linear inverse problems, *IEEE Trans. Biomed. Eng.* 53 (9) (2006) 1775–1782.
- [27] F.A. Dahlen, F.J. Simons, Spectral estimation on a sphere in geophysics and cosmology, *Geophys. J. Int.* 174 (3) (2008) 774–807.
- [28] S. Das, A. Hajian, D.N. Spergel, Efficient power spectrum estimation for high resolution CMB maps, *Phys. Rev. D* 79 (8) (2009) 083008.
- [29] C. Lessig, E. Fiume, On the effective dimension of light transport, in: J. Lawrence, M. Stamminger (Eds.), *Eurographics Symposium on Rendering 2010*, vol. 29 (4), The Eurographics Association, 2010, pp. 1399–1403, <http://dx.doi.org/10.1111/j.1467-8659.2010.01736.x>.
- [30] B.T.T. Yeo, W. Ou, P. Golland, On the construction of invertible filter banks on the 2-sphere, *IEEE Trans. Image Process.* 17 (3) (2008) 283–300, <http://dx.doi.org/10.1109/TIP.2007.915550>.
- [31] I. SenGupta, B. Sun, W. Jiang, G. Chen, M.C. Mariani, Concentration problems for bandpass filters in communication theory over disjoint frequency intervals and numerical solutions, *J. Fourier Anal. Appl.* 18 (2012) 182–210, <http://dx.doi.org/10.1007/s00041-011-9197-y>.
- [32] Z. Khalid, S. Durrani, P. Sadeghi, R.A. Kennedy, Spatio-spectral analysis on the sphere using spatially localized spherical harmonics transform, *IEEE Trans. Signal Process.* 60 (3) (2012) 1487–1492, <http://dx.doi.org/10.1109/TSP.2011.2177265>.
- [33] L. Wei, R.A. Kennedy, T.A. Lamahewa, Quadratic variational framework for signal design on the 2-sphere, *IEEE Trans. Signal Process.* 59 (11) (2011) 5243–5252, <http://dx.doi.org/10.1109/TSP.2011.2162506>.
- [34] D. Marinucci, G. Peccati, Representations of SO(3) and angular polyspectra, *J. Multivariate Anal.* 191 (2010) 77–100, <http://dx.doi.org/10.1016/j.jmva.2009.04.017>.
- [35] V. Michel, Optimally localized approximate identities on the 2-sphere, *Numer. Funct. Anal. Optim.* 32 (8) (2011) 877–903, <http://dx.doi.org/10.1080/01630563.2011.587073>.
- [36] P.P. Mitra, H. Maniar, Local basis expansions for MEG source localization, *Int. J. Bioelectromagn.* 7 (2) (2005) 30–33.
- [37] M. Eshagh, Spatially restricted integrals in gradiometric boundary value problems, *Artif. Satell.* 44 (4) (2009) 131–148, <http://dx.doi.org/10.2478/v10018-009-0025-4>.
- [38] R. Stockmann, C.C. Finlay, A. Jackson, Imaging Earth's crustal magnetic field with satellite data: A regularized spherical triangle tessellation approach, *Geophys. J. Int.* 179 (2) (2009) 929–944, <http://dx.doi.org/10.1111/j.1365-246X.2009.04345.x>.
- [39] D. Gubbins, D. Ivers, S.M. Masterton, D.E. Winch, Analysis of lithospheric magnetization in vector spherical harmonics, *Geophys. J. Int.* 187 (2011) 99–117, <http://dx.doi.org/10.1111/j.1365-246X.2011.05153.x>.
- [40] E. Friis-Christensen, H. Luhr, G. Hulot, Swarm: A constellation to study the Earth's magnetic field, *Earth Planets Space* 58 (4) (2006) 351–358.
- [41] L. Shure, R.L. Parker, G.E. Backus, Harmonic splines for geomagnetic modeling, *Phys. Earth Planet. Inter.* 28 (3) (1982) 215–229.
- [42] R.L. Parker, L. Shure, Efficient modeling of the Earth's magnetic field with harmonic splines, *Geophys. Res. Lett.* 9 (8) (1982) 812–815.

- [43] R.A. Langel, The main field, in: J. Jacobs (Ed.), *Geomagnetism*, vol. 1, Academic Press, London, 1987, pp. 249–512.
- [44] G.V. Haines, Spherical cap harmonic analysis, *J. Geophys. Res.* 90 (NB3) (1985) 2583–2591.
- [45] A. De Santis, Translated origin spherical cap harmonic analysis, *Geophys. J. Int.* 106 (1) (1991) 253–263.
- [46] M. Korte, R. Holme, Regularization of spherical cap harmonics, *Geophys. J. Int.* 153 (1) (2003) 253–262.
- [47] E. Thébault, Global lithospheric magnetic field modelling by successive regional analysis, *Earth Planets Space* 58 (4) (2006) 485–495.
- [48] E. Thébault, J.J. Schott, M. Mandea, Revised spherical cap harmonic analysis (R-SCHA): Validation and properties, *J. Geophys. Res.* 111 (B1) (2006) B01102, <http://dx.doi.org/10.1029/2005JB003836>.
- [49] M. Holschneider, A. Chambodut, M. Mandea, From global to regional analysis of the magnetic field on the sphere using wavelet frames, *Phys. Earth Planet. Inter.* 135 (2003) 107–124.
- [50] A. Chambodut, I. Panet, M. Mandea, M. Diamant, M. Holschneider, O. Jamet, Wavelet frames: An alternative to spherical harmonic representation of potential fields, *Geophys. J. Int.* 163 (3) (2005) 875–899.
- [51] C. Mayer, T. Maier, Separating inner and outer Earth's magnetic field from CHAMP satellite measurements by means of vector scaling functions and wavelets, *Geophys. J. Int.* 167 (2006) 1188–1203.
- [52] F.A. Dahlen, J. Tromp, *Theoretical Global Seismology*, Princeton Univ. Press, Princeton, NJ, 1998.
- [53] J. Jeans, The propagation of earthquake waves, *Philos. Trans. R. Soc. Lond. Ser. A Math. Phys. Eng. Sci.* 102 (1923) 554–574.
- [54] A.R. Edmonds, *Angular Momentum in Quantum Mechanics*, Princeton Univ. Press, Princeton, NJ, 1996.
- [55] A. Messiah, *Quantum Mechanics*, Dover, New York, 2000.
- [56] K.H. Ilk, Ein Beitrag zur Dynamik ausgedehnter Körper: Gravitationswechselwirkung, *Dtsch. Geod. Komm.* C 288 (1983).
- [57] M.K. Paul, Recurrence relations for integrals of associated Legendre functions, *Bull. Geod.* 52 (1978) 177–190.
- [58] W. Freedman, M. Schreiner, *Spherical Functions of Mathematical Geosciences: A Scalar, Vectorial, and Tensorial Setup*, Springer-Verlag, Berlin, Heidelberg, 2009.
- [59] D. Slepian, Prolate spheroidal wave functions, Fourier analysis and uncertainty – IV: Extensions to many dimensions; generalized prolate spheroidal functions, *Bell Syst. Tech. J.* 43 (6) (1964) 3009–3057.
- [60] R.A. Horn, C.R. Johnson, *Matrix Analysis*, Cambridge University Press, Cambridge, UK, 1990.
- [61] F.G. Tricomi, *Integral Equations*, 5th edition, Interscience, New York, 1970.
- [62] H.J. Landau, On the eigenvalue behavior of certain convolution equations, *Trans. Amer. Math. Soc.* 115 (1965) 242–256.
- [63] H.J. Landau, Necessary density conditions for sampling and interpolation of certain entire functions, *Acta Math.* 117 (1) (1967) 37–52.
- [64] P. Flandrin, *Time–Frequency/Time–Scale Analysis*, Academic Press, San Diego, CA, 1999.
- [65] R.P. Kanwal, *Linear Integral Equations: Theory and Technique*, Academic Press, New York, 1971.
- [66] M.A. Blanco, M. Flórez, M. Bermejo, Evaluation of the rotation matrices in the basis of real spherical harmonics, *J. Mol. Struct., Theochem* 419 (1997) 19–27.
- [67] M.A. Wiczorek, F.J. Simons, Localized spectral analysis on the sphere, *Geophys. J. Int.* 162 (3) (2005) 655–675, <http://dx.doi.org/10.1111/j.1365-246X.2005.02687.x>.
- [68] D.B. Percival, A.T. Walden, *Spectral Analysis for Physical Applications, Multitaper and Conventional Univariate Techniques*, Cambridge University Press, New York, 1993.
- [69] D. Slepian, E. Sonnenblick, Eigenvalues associated with prolate spheroidal wave functions of zero order, *Bell Syst. Tech. J.* 44 (1965) 1745–1759.
- [70] S. Maus, H. Luhr, M. Purucker, Simulation of the high-degree lithospheric field recovery for the Swarm constellation of satellites, *Earth Planets Space* 58 (4) (2006) 397–407.
- [71] C.D. Beggan, J. Saarimäki, K.A. Whaler, F.J. Simons, Spectral and spatial decomposition of lithospheric magnetic field models using spherical Slepian functions, *Geophys. J. Int.* (2013), <http://dx.doi.org/10.1093/gji/ggs122>, in press.
- [72] T.J. Sabaka, N. Olsen, Enhancing comprehensive inversions using the Swarm constellation, *Earth Planets Space* 58 (4) (2006) 371–395.
- [73] B. Langlais, V. Lesur, M.E. Purucker, J.E.P. Connerney, M. Mandea, Crustal magnetic fields of terrestrial planets, *Space Sci. Rev.* 152 (1) (2010) 223–249.
- [74] K.W. Lewis, F.J. Simons, Local spectral variability and the origin of the Martian crustal magnetic field, *Geophys. Res. Lett.* 39 (2012) L18201, <http://dx.doi.org/10.1029/2012GL052708>.
- [75] M.G. Sterenborg, J. Bloxham, Application of Slepian basis functions to magnetic field analysis of Saturn, in: *Eos Trans. AGU, Fall Meet. Suppl., Abstract G0P33A-0928*, 2007.
- [76] S. Maus, An ellipsoidal harmonic representation of Earth's lithospheric magnetic field to degree and order 720, *Geochem. Geophys. Geosyst.* 11 (2010) 06015, <http://dx.doi.org/10.1029/2010GC003026>.
- [77] R. Schachtschneider, M. Holschneider, M. Mandea, Error distribution in regional inversion of potential field data, *Geophys. J. Int.* 181 (2010) 1428–1440, <http://dx.doi.org/10.1111/j.1365-246X.2010.04598.x>.
- [78] R. Schachtschneider, M. Holschneider, M. Mandea, Error distribution in regional modelling of the geomagnetic field, *Geophys. J. Int.* 191 (2012) 1015–1024, <http://dx.doi.org/10.1111/j.1365-246X.2012.05675.x>.
- [79] K. Jahn, N. Bokor, Vector Slepian basis functions with optimal energy concentration in high numerical aperture focusing, *Opt. Commun.* 285 (8) (2012) 2028–2038, <http://dx.doi.org/10.1016/j.optcom.2011.11.107>.